European Journal of Mechanics / A Solids 117 (2026) 106003

Contents lists available at ScienceDirect

European Journal of Mechanics / A Solids

journal homepage: www.elsevier.com/locate/ejmsol

Full length article

Partial and Lamb waves in non-local elasticity with kernel modification

Dipendu Pramanik [a], Andrea Nobili [a,b,*], Santanu Manna [c]

[a] Department of Engineering Enzo Ferrari, University of Modena and Reggio Emilia, via Vivarelli 10, 41125, Modena, Italy
[b] National Group for Mathematical Physics (GNFM), Institute for Higher Mathematics Francesco Severi (INdAM), Piazzale Aldo Moro, 5, 00185, Rome, Italy
[c] Department of Mathematics, Indian Institute of Technology Indore, Khandwa Rd, Simrol, 453552, Indore, Madhya Pradesh, India

ARTICLE INFO

Keywords:
Rayleigh–Lamb waves
Non-local theory
Well-posedness
Kernel modification
Constitutive boundary conditions

ABSTRACT

We study dispersion of Rayleigh–Lamb (R-L) waves in an infinite isotropic strip within the theory of non-local elasticity with kernel modification. Within this approach, the set of constitutive boundary conditions (CBCs) embedded in the attenuation functions contain the set of natural boundary conditions (BCs) of the problem and this feature, besides avoiding nonphysical BCs, warrants that the problem is well-posed. We show that, in contrast to local elasticity, the dispersion equation emerges from imposing the equations of motion, given that the BCs are automatically satisfied by the very choice of the attenuation functions. Similarly to local elasticity, the problem naturally decouples into symmetric and anti-symmetric partial modes, although this feature is not obvious here and crucially depends on certain symmetry properties of the kernels. We prove that symmetric and anti-symmetric kernels may be constructed directly, to avoid solving the full problem, and we show how these kernels relate to the original. Explicit dispersion relations for symmetric and anti-symmetric partial waves are obtained, that reveal the size-dependent deviation from the classical predictions. Overall, results reproduce the general features already observed in local elasticity, such as the convergence of the fundamental modes to the Rayleigh speed and of the higher modes to the bulk wave speeds, although these are no longer constants. Yet, both fundamental modes, and especially the symmetric one, significantly depart from the local theory, which fact has important consequences on the corresponding asymptotic model for non-local beams.

1. Introduction

The classical theory of linear elasticity provides an exceptionally successful framework for analysing macroscopic solid mechanics problems. However, at length scales comparable to microstructural features, such as in thin films, layered nanostructures, and architected materials, the assumption of locality breaks down. Experimental and numerical evidence consistently demonstrates size-dependent effects that cannot be captured by classical continuum models (Karlicic et al., 2015; Zima and Kędra, 2020). To address these shortcomings, Kröner (1967) and later Eringen and Edelen (1972) introduced the theory of non-local elasticity, in which the stress at a point depends not only on the local strain but also on the strain field in its finite (as opposed to infinitesimal) neighbourhood. By embedding an internal material length scale, non-local models are able to predict dispersion, finite stress at the crack tip, and size-dependent stiffening or softening phenomena (Eringen, 1972; Eringen and Kim, 1974; Eringen, 2002) observed in nanoscale and micro-structured materials, and are therefore increasingly used in the modelling of nano-systems, thin films, and metamaterials.

Despite its promises, the classical non-local formulation exhibits well-documented shortcomings that often lead to the lack of solutions or to paradoxes. They may be all traced to the fact that, in its integral form, the constitutive law involves a spatial convolution kernel (attenuation function) defined over the entire domain. To simplify its use and facilitate analytical work, an equivalent differential representation was proposed by Eringen (1983), in the form of a Helmholtz-type operator. However, the differential form is not strictly equivalent for bounded domains, equivalence requiring the introduction of constitutive boundary conditions (CBCs) on the non-local stress field that ensure compatibility between the integral and differential representations. If these CBCs are neglected, or if local boundary conditions are incorrectly applied to the non-local stress, the resulting boundary-value problem may become over-determined or physically inconsistent. Kaplunov et al. (2023) recently highlighted this issue, showing the non-equivalence between the integral and the differential formulation and the consequent ill-posed character of the boundary-value problem. Further studies by Kaplunov et al. (2022) and Pham and Vu (2024) have attempted to regularize this inconsistency through asymptotic or differential techniques. In contrast, our recent contributions (Nobili and Pramanik, 2025a,b; Pramanik and Nobili, 2025) systematically addressed this ill-posedness by modifying the attenuation functions so that the physical (natural)

* Corresponding author at: Department of Engineering Enzo Ferrari, University of Modena and Reggio Emilia, via Vivarelli 10, 41125, Modena, Italy.
E-mail address: andrea.nobili@unimore.it (A. Nobili).

https://doi.org/10.1016/j.euromechsol.2025.106003
Received 3 November 2025; Received in revised form 11 December 2025; Accepted 15 December 2025
Available online 16 December 2025

boundary conditions are contained within the set of the CBCs. Interestingly, the necessity to go beyond the standard convolution-type attenuation function was already recognized by Eringen (1984, §9) in connection with the Rayleigh problem: "Half-space ceases to be homogeneous in the vicinity of the surface $x_2 = 0$, where [...] the material is inhomogeneous and therefore a perturbation is necessary to $\alpha(\|\boldsymbol{x}-\boldsymbol{\xi}\|)$". The kernel-modification strategy ensures both mathematical well-posedness and energetic admissibility, which are fundamental for physically consistent non-local models in one- and two-dimensional settings.

Guided elastic waves in plates with traction-free surfaces, commonly known as Rayleigh–Lamb (R-L) waves were first analysed by Lamb (1917). These waves play a central role in understanding elastic wave propagation in bounded media and are widely used in non-destructive testing, structural health monitoring, and ultrasonic metrology, owing to their sensitivity to geometry, material parameters, and boundary conditions (Graff, 2012; Achenbach, 2012). At micro- and nano-scales, or in engineered materials such as phononic crystals, thin coatings, and layered composites, microstructural effects substantially alter the dispersion, attenuation, and mode shapes of guided waves. To interpret such effects quantitatively, non-local constitutive models are essential, making the extension of R-L theory to non-local elasticity both fundamentally and practically significant.

Many contributions have appeared in the literature dealing with the interpretation of the R-L spectrum within classical local elasticity, e.g. Ryden et al. (2003), Royer et al. (2009), Kuznetsov (2014). In particular, Mindlin (1960) and Solie and Auld (1973) demonstrated that R-L waves can be decomposed into symmetric and anti-symmetric partial modes through appropriate mid-plane boundary conditions, while Nobili et al. (2022) studied veering of these partial modes. Extensions of these results have been proposed in many directions, for example in materials with voids (Chandrasekharaiah, 1987; Kumar and Tomar, 2022) or in weakly non-local materials, where non-locality is considered in the close neighbourhood of the point of interest, such it is the case in the couple-stress theory (Nobili et al., 2020; Nobili, 2021). Conversely, only a handful of studies have analysed the R-L spectrum within the non-local elasticity theory, probably in view of the difficulties attached to properly incorporating the problem BCs. As a case in point, Thi Ngoc Anh et al. (2025) recently investigated guided waves in composite plates using a weakly non-local model and yet they applied *local* BCs. Exactly the same seemingly inconsistent approach can be found in Kaur et al. (2021). The present study addresses these issues by developing a kernel-modified non-local elasticity framework that enforces compatibility between constitutive and natural boundary conditions for a finite elastic strip. Building on our earlier kernel-modification approach (Nobili and Pramanik, 2025a,b; Pramanik and Nobili, 2025), we construct Green's function kernels that vanish at the strip surfaces, thereby generating CBCs consistent with traction-free boundaries. Using the differential (Helmholtz) formulation alongside the integral representation of these modified Green's functions, we derive closed-form non-local stress fields and explicit dispersion relations for symmetric and anti-symmetric R-L modes. The results reveal size-dependent phase velocity shifts, curvature variations, and reductions in the number of propagating modes, while also clarifying how Poisson's ratio influences higher-order branches. Moreover, we establish a new identity demonstrating the equivalence between the image-series and Fourier-integral representations of the modified kernel, highlighting the physical implications of boundary-adapted kernels in non-local models.

The remainder of this paper is organized as follows. Section 2 formulates the problem and reviews the integral and differential representations of the non-local stress field. Section 3 presents the solution methodology, non-local stress distributions, and the general dispersion relations. Section 4 discusses the symmetric and anti-symmetric partial waves together with their associated kernels, while Section 5 provides numerical illustrations of their dispersion behaviour. Appendix A gives the image-series and integral representations of the modified kernels. Finally, Section 6 concludes the paper with remarks and perspectives.

2. Problem formulation

Let us consider a homogeneous isotropic linearly elastic infinite strip with thickness $2h$, under plane strain conditions. A Cartesian coordinate system (x_1, x_3) is introduced such that the x_1-axis is directed along the propagation direction, while x_3 lies across, in the thickness direction, and the strip occupies the plane region $\mathbb{V} = \{(x_1, x_3) : -h \le x_3 \le h\}$. We introduce the non-zero displacement components

$$u_1 = u_1(\boldsymbol{x}, t), \quad u_3 = u_3(\boldsymbol{x}, t), \tag{1}$$

which depend on the position, $\boldsymbol{x} = [x_1, x_3]$, as well as on time t. Alongside displacements, we let the non-local stress components t_{ij}, $i, j \in \{1, 3\}$, which differ from the classical (local) stresses σ_{ij}. Indeed, following Eringen (1972), non-local stresses are expressed as the weighted spatial average of the local counterparts through the *attenuation function* (kernel) $\alpha_{ij}(\boldsymbol{x}, \boldsymbol{\xi})$, i.e.

$$t_{ij}(\boldsymbol{x}, t) = \int_{\mathbb{V}} \alpha_{ij}(\boldsymbol{x}, \boldsymbol{\xi})\, \sigma_{ij}(\boldsymbol{\xi}, t)\, \mathrm{d}\boldsymbol{\xi}, \quad \boldsymbol{x}, \boldsymbol{\xi} \in \mathbb{V}, \quad \text{(no summation)}, \tag{2}$$

where $\mathrm{d}\boldsymbol{\xi} = \mathrm{d}\xi_1 \mathrm{d}\xi_3$ denotes the differential area element. Attenuation functions are generally different for different stress components and their choice is only constrained by some fundamental requirements, such as impulsivity (presently defined), unity (which is a form of normalization) and reciprocity (that warrants a symmetric energy density). For the sake of definiteness, and again following Eringen, we define the attenuation functions as the Green's function of the Helmholtz operator

$$\mathfrak{L} = 1 - \epsilon^2 \nabla^2, \tag{3}$$

where $\nabla^2 = \frac{\partial^2}{\partial x_1^2} + \frac{\partial^2}{\partial x_3^2}$ is the two-dimensional Laplacian operator. The operator involves the characteristic internal length $\epsilon > 0$, which governs the spatial range of the non-local interaction and indeed represents the stress-diffusion length scale. By the impulsivity requirement, one demands that, in the limit as $\epsilon \to 0$, the kernel reduces to Dirac's delta distribution, i.e., $\lim_{\epsilon \to 0} \alpha_{ij}(\boldsymbol{x}, \boldsymbol{\xi}) = \delta(\boldsymbol{x} - \boldsymbol{\xi})$, thereby recovering the classical theory of local elasticity. Application of the operator $\mathfrak{L}$ to (2) while accounting for the fact that the kernel $\alpha_{ij}(\boldsymbol{x}, \boldsymbol{\xi})$ is the Green's function for the operator $\mathfrak{L}$, i.e., $\mathfrak{L}\alpha_{ij}(\boldsymbol{x}, \boldsymbol{\xi}) = \delta(\boldsymbol{x} - \boldsymbol{\xi})$, yields

$$\mathfrak{L} t_{ij} = \sigma_{ij}, \quad i, j \in \{1, 3\}\,. \tag{4}$$

It is important to emphasize that specification of the differential operator alone is not sufficient to fully define the Green's function, and, equally, the kernel. Indeed, the differential operator (4) needs to be supplemented by additional boundary requirements, often referred to as *constitutive boundary conditions* (CBCs), which are embedded in the corresponding attenuation function. As illustrated in the literature, e.g. Pham and Vu (2024), the unguided (or unaware) selection of the CBCs most often leads to an over-determined formulation, for CBCs stand in excess of the natural boundary conditions (BCs) attached to the physical problem and, as a result, the problem becomes ill-posed. In contrast, Nobili and Pramanik (2025b,a), Pramanik and Nobili (2025) proposed to set the CBCs according to the BCs, in a procedure named *kernel modification*. Within this approach, the problem becomes well-posed and its solution may be found. In this paper, we follow this very approach and adopt the natural BCs of the problem, that demand that boundaries are traction-free at the strip faces, as belonging to the set of CBCs,

$$t_{13} = t_{33} = 0, \quad \text{at} \quad x_3 = \pm h. \tag{5}$$

It is emphasized that, within a consistent approach, the BCs (5) are expressed in terms of the non-local stresses, which fact is often overlooked in the literature where local stresses are used instead. Besides, it is observed that the available BCs (5) are insufficient for the full determination of the required three attenuation functions, and, in fact, α_{11} remains undefined. In other words, adopting the BCs do not exhaust

the choice of the available CBCs. To complete the kernel definition, we decide to warrant symmetric (homogeneous) decay as $x_1 \to \pm\infty$ and accordingly set $\alpha_{11}(\boldsymbol{x},\boldsymbol{\xi})$ as the zeroth-order Bessel function of the second kind, $K_0(\epsilon^{-1}\|\boldsymbol{x}-\boldsymbol{\xi}\|)$, where $\|\boldsymbol{x}\|$ denotes the Euclidean norm, i.e. $\|\boldsymbol{x}\| = \sqrt{x_1^2+x_3^2}$. The problem formulation is completed by prescribing the local stresses σ_{ij} through Hooke's law

$$\left.\begin{aligned}\sigma_{11} &= (\lambda+2\mu)\,\frac{\partial u_1}{\partial x_1} + \lambda\frac{\partial u_3}{\partial x_3},\\ \sigma_{13} &= \mu\left(\frac{\partial u_1}{\partial x_3} + \frac{\partial u_3}{\partial x_1}\right),\\ \sigma_{33} &= (\lambda+2\mu)\,\frac{\partial u_3}{\partial x_3} + \lambda\frac{\partial u_1}{\partial x_1},\end{aligned}\right\} \tag{6}$$

with λ and μ denoting the Lamé constants of the material. Once the local stresses are obtained from (6), the problem formulation may be completed by following either the integral approach, that is making use of (2), or the differential approach, namely recalling (4). In either case, allowing for sufficient regularity, results coincide, provided that full account is taken of the CBCs. Indeed, failure to account for the CBCs in the differential formulation stands at the root of many misconceptions, most notably the idea that formulations are not equivalent and that only the differential approach is meaningful, see, among many, Kaplunov et al. (2022, 2023). If a difference should be made between the integral and the differential formulation, preference should go to the former, given that the integral approach is capable of dealing with "pathologic" (non-smooth) local stresses which are intractable by the differential approach.

3. Rayleigh–Lamb waves

We now seek plane wave solutions travelling along the strip, which form the well-known Rayleigh–Lamb wave set, see Graff (2012, §8.1.3). For this, we write the balance of linear momentum, in the absence of body forces (ρ is the mass density),

$$\frac{\partial t_{11}}{\partial x_1} + \frac{\partial t_{31}}{\partial x_3} = \rho\frac{\partial^2 u_1}{\partial t^2}, \quad \frac{\partial t_{13}}{\partial x_1} + \frac{\partial t_{33}}{\partial x_3} = \rho\frac{\partial^2 u_3}{\partial t^2}, \tag{7}$$

and to both sides of these equations we apply the operator $\mathfrak{L}$. This step, however, introduces spurious solutions, on account of the differentiation process. Making use of the differential constitutive relation (4), we obtain the modified system

$$\left.\begin{aligned}\frac{\partial\sigma_{11}}{\partial x_1} + \frac{\partial\sigma_{31}}{\partial x_3} &= \rho\left(1-\epsilon^2\nabla^2\right)\frac{\partial^2 u_1}{\partial t^2}\\ \frac{\partial\sigma_{13}}{\partial x_1} + \frac{\partial\sigma_{33}}{\partial x_3} &= \rho\left(1-\epsilon^2\nabla^2\right)\frac{\partial^2 u_3}{\partial t^2}\end{aligned}\right\}, \tag{8}$$

where we see that the new motion equations in the local stresses introduce the concept of *modified inertia*. Upon substituting the classical stress–displacement relations (6), we arrive at a coupled system of PDEs that are the counterpart of the Navier equations of classical elasticity

$$\left.\begin{aligned}c_1^2\frac{\partial^2 u_1}{\partial x_1^2} + \left(c_1^2-c_2^2\right)\frac{\partial^2 u_3}{\partial x_1\partial x_3} + c_2^2\frac{\partial^2 u_1}{\partial x_3^2} &= \left(1-\epsilon^2\nabla^2\right)\frac{\partial^2 u_1}{\partial t^2},\\ \left(c_1^2-c_2^2\right)\frac{\partial^2 u_1}{\partial x_1\partial x_3} + c_2^2\frac{\partial^2 u_3}{\partial x_1^2} + c_1^2\frac{\partial^2 u_3}{\partial x_3^2} &= \left(1-\epsilon^2\nabla^2\right)\frac{\partial^2 u_3}{\partial t^2},\end{aligned}\right\} \tag{9}$$

where $c_1 = \sqrt{(\lambda+2\mu)/\rho}$ and $c_2 = \sqrt{\mu/\rho}$ are the classical longitudinal and shear wave speeds, respectively. Hereinafter, we let the bulk wave speed ratio $\kappa = c_1/c_2 > 1$.

3.1. Travelling wave solution

We now restrict attention to harmonic disturbances, where all field quantities are assumed to vary sinusoidally in the propagation direction x_1 and in time t:

$$\left\{u_i,\sigma_{ij},t_{ij}\right\}(x_1,x_3,t) = \left\{U_i,S_{ij},T_{ij}\right\}(x_3)\,e^{\imath k(x_1-ct)}, \quad i,j=1,3, \tag{10}$$

where k is the wavenumber along x_1, c is the phase velocity and $\imath^2=-1$.

Substituting (10) into (9), we reduce the governing equations to a coupled system of ordinary differential equations (ODEs)

$$\left.\begin{aligned}\left(1-k_1^2\epsilon_1^2\upsilon^2\right)U_1'' + k^2\left\{\upsilon^2(1+k_1^2\epsilon_1^2)-\kappa^2\right\}U_1 + \imath k\left(\kappa^2-1\right)U_3' = 0,\\ \left(\kappa^2-k_1^2\epsilon_1^2\upsilon^2\right)U_3'' + k^2\left\{\upsilon^2(1+k_1^2\epsilon_1^2)-1\right\}U_3 + \imath k\left(\kappa^2-1\right)U_1' = 0,\end{aligned}\right\} \tag{11}$$

where we have introduced the dimensionless wavenumber $k_1 = kh$, the relative non-local parameter $\epsilon_1 = \epsilon/h$ and the dimensionless phase velocity $\upsilon = c/c_2$. This system of ODEs admits exponential-type solutions across the strip thickness which, after standard algebraic manipulations, lend the general solution for the displacement amplitudes

$$\left.\begin{aligned}U_1(x_3) &= k^{-1}\left[A_1e^{-kb_1x_3} + A_2e^{kb_1x_3} + A_3e^{-kb_2x_3} + A_4e^{kb_2x_3}\right],\\ U_3(x_3) &= \imath k^{-1}\left[b_1A_1e^{-kb_1x_3} - b_1A_2e^{kb_1x_3} + \frac{A_3}{b_2}e^{-kb_2x_3} - \frac{A_4}{b_2}e^{kb_2x_3}\right],\end{aligned}\right\} \tag{12}$$

where $A_i (i=1,2,3,4)$ are dimensionless arbitrary constants, and we have let the dimensionless wavenumbers in the thickness direction for bulk waves (often named decay indices), see Nobili and Pramanik (2025a, Eq.(17)),

$$b_1 = \sqrt{1-\frac{\upsilon^2}{\kappa^2-k_1^2\epsilon_1^2\upsilon^2}}, \quad b_2 = \sqrt{1-\frac{\upsilon^2}{1-k_1^2\epsilon_1^2\upsilon^2}}. \tag{13}$$

In Eqs. (13), the branch cut of the square root is chosen so that $\sqrt{x}$ is real, which requirement gives the hyperbolic branch cuts described in Graff (2012, §6.2.2). Within this convention, a pair of real-valued decay indices exists whenever $\upsilon < \upsilon_S \equiv 1/b_3$, where υ_S is the dimensionless shear bulk wave speed in non-local elasticity and we have let the shorthand

$$b_3 = \sqrt{1+k_1^2\epsilon_1^2}. \tag{14}$$

As it can be easily seen, unlike local elasticity, the bulk shear wave speed υ_S is not constant and in fact it closely matches "the dispersion curve for the Born–Karraan model of lattice dynamics" (Eringen, 1984, §9). Similarly, we define the dimensionless longitudinal bulk wave speed $\upsilon_L = \kappa/b_3 > \upsilon_S$. Plugging Eqs. (12) into Eqs. (6), the amplitude of the local stress components σ_{ij} is immediately obtained

$$\left.\begin{aligned}S_{11}(x_3) &= \imath\mu\left[P_1\left(A_1e^{-kb_1x_3} + A_2e^{kb_1x_3}\right) + Q_1\left(A_3e^{-kb_2x_3} + A_4e^{kb_2x_3}\right)\right],\\ S_{13}(x_3) &= \mu\left[P_2\left(A_1e^{-kb_1x_3} - A_2e^{kb_1x_3}\right) + Q_2\left(A_3e^{-kb_2x_3} - A_4e^{kb_2x_3}\right)\right],\\ S_{33}(x_3) &= \imath\mu\left[P_3\left(A_1e^{-kb_1x_3} + A_2e^{kb_1x_3}\right) + Q_3\left(A_3e^{-kb_2x_3} + A_4e^{kb_2x_3}\right)\right],\end{aligned}\right\} \tag{15}$$

where (cfr. Nobili and Pramanik (2025a, Eq.(19)))

$$\left.\begin{aligned}&P_1 = \kappa^2-\left(\kappa^2-2\right)b_1^2, \quad P_2 = -2b_1, \quad P_3 = \kappa^2(1-b_1^2)-2,\\ &Q_1 = -Q_3 = 2, \quad Q_2 = -\tfrac{1+b_2^2}{b_2}.\end{aligned}\right\} \tag{16}$$

3.2. Construction of non-local stress components

To determine the non-local stress components $t_{ij}\,(i,j=1,3)$ using the kernel modification method, it is first necessary to specify suitable attenuation functions α_{ij}. The choice of these functions must ensure that the constitutive boundary conditions (CBCs) generated by the non-local formulation remain consistent with the traction-free natural boundary conditions (5). Such requirement uniquely sets the attenuation functions

$$\alpha_{13}(x_1,x_3;\xi_1,\xi_3) = \alpha_{33}(x_1,x_3;\xi_1,\xi_3) = G_2(x_1,x_3;\xi_1,\xi_3), \tag{17}$$

where the Green's function G_2 is defined as

$$G_2(x_1,x_3;\xi_1,\xi_3) =$$

$$\frac{1}{4\pi\epsilon^2}\int \frac{\cosh\left[\beta\left(2h-|x_3-\xi_3|\right)\right]-\cosh\left[\beta\left(x_3+\xi_3\right)\right]}{\beta\sinh(2\beta h)}e^{-\imath s(x_1-\xi_1)}\mathrm{d}s. \tag{18}$$

Appendix A presents a derivation of this Green's function based on the integral transform technique, as well as a second derivation of an equivalent expression, this time obtained by the method of images, see Eqs. (A.14), (A.16). Yet, it is noted that a simpler approach is available that splits the problem into symmetric and anti-symmetric partial waves: this procedure is described in Section 4.

As already anticipated, for the longitudinal stress component t_{11}, no natural BC is available to fix the relevant attenuation function $\alpha_{11}(\boldsymbol{x},\boldsymbol{\xi})$, which therefore rests indeterminate, at least in terms of CBCs (but not in terms of the underlying operator, that remains defined as $\mathfrak{L}$). In this case, we decide to adopt the zeroth order Bessel function of the second kind

$$\alpha_{11}(x_1,x_3;\xi_1,\xi_3)=\frac{1}{2\pi\epsilon^2}K_0\left(\epsilon^{-1}\sqrt{(x_1-\xi_1)^2+(x_3-\xi_3)^2}\right), \tag{19}$$

which, physically, amounts to choosing radially symmetric decay. Consequently, this attenuation function takes the form of a difference kernel and the integral (2) becomes of the convolution-type. The corresponding CBCs, that exist, although they are not apparent, are not required here, because they are automatically enforced by the integral method. Conversely, they are required for the application of the differential method and, for the sake of completeness, they are presented in Eq. (A.8). It is very important to remark that, alongside the already mentioned impulsivity, unity and reciprocity properties, both kernels (18) and (19) enjoy the *point-symmetry property*

$$G(\boldsymbol{x},\boldsymbol{\xi})=G(-\boldsymbol{\xi},-\boldsymbol{x}) \tag{20}$$

that proves essential for the splitting procedure described in Section 4. In fact, symmetry holds in the stronger sense of *mirror symmetry*, e.g.

$$G(x_1,x_3,\xi_1,\xi_3)=G(x_1,-\xi_3,\xi_1,-x_3),\quad G(x_1,x_3,\xi_1,\xi_3)=G(-\xi_1,x_3,-x_1,\xi_3). \tag{21}$$

The non-local stress components are obtained from (2)

$$t_{ij}(x_1,x_3,t)=\int_{-h}^{h}\mathrm{d}\xi_3\int_{-\infty}^{\infty}\alpha_{ij}\left(x_1,x_3;\xi_1,\xi_3\right)\sigma_{ij}(\xi_1,\xi_3,t)\mathrm{d}\xi_1,\quad i,j\in\{1,3\}, \tag{22}$$

where, making use of their integral representations Eq. (18) and (A.2), together with the explicit expressions of the local stress components Eqs. (15), the integrals can be evaluated in closed form. Indeed, explicit expressions for the non-local stress components are obtained

$$\begin{aligned}T_{11}(x_3)=\imath\mu\Bigg[&P_1\frac{A_1e^{-kb_1x_3}+A_2e^{kb_1x_3}}{b_3^2-k_1^2\epsilon_1^2b_1^2}+Q_1\frac{A_3e^{-kb_2x_3}+A_4e^{kb_2x_3}}{b_3^2-k_1^2\epsilon_1^2b_2^2}\\&-\frac{1}{2b_3}e^{-\frac{b_3}{\epsilon}(x_3+h)}\left(\frac{P_{11}P_1}{b_3^2-k_1^2\epsilon_1^2b_1^2}+\frac{Q_{11}Q_1}{b_3^2-k_1^2\epsilon_1^2b_2^2}\right)\\&-\frac{1}{2b_3}e^{\frac{b_3}{\epsilon}(x_3-h)}\left(\frac{P_{12}P_1}{b_3^2-k_1^2\epsilon_1^2b_1^2}+\frac{Q_{12}Q_1}{b_3^2-k_1^2\epsilon_1^2b_2^2}\right)\Bigg],\end{aligned} \tag{23a}$$

$$\begin{aligned}T_{13}(x_3)=\mu\Bigg[&P_2\frac{A_1e^{-kb_1x_3}-A_2e^{kb_1x_3}}{b_3^2-k_1^2\epsilon_1^2b_1^2}+Q_2\frac{A_3e^{-kb_2x_3}-A_4e^{kb_2x_3}}{b_3^2-k_1^2\epsilon_1^2b_2^2}\\&-e^{-\frac{b_3}{\epsilon}x_3}\operatorname{cosech}\left(\frac{2b_3}{\epsilon_1}\right)\left(\frac{P_{21}P_2}{b_3^2-k_1^2\epsilon_1^2b_1^2}+\frac{Q_{21}Q_2}{b_3^2-k_1^2\epsilon_1^2b_2^2}\right)\\&+e^{\frac{b_3}{\epsilon}x_3}\operatorname{cosech}\left(\frac{2b_3}{\epsilon_1}\right)\left(\frac{P_{22}P_2}{b_3^2-k_1^2\epsilon_1^2b_1^2}+\frac{Q_{22}Q_2}{b_3^2-k_1^2\epsilon_1^2b_2^2}\right)\Bigg],\end{aligned} \tag{23b}$$

$$\begin{aligned}T_{33}(x_3)=\imath\mu\Bigg[&P_3\frac{A_1e^{-kb_1x_3}+A_2e^{kb_1x_3}}{b_3^2-k_1^2\epsilon_1^2b_1^2}+Q_3\frac{A_3e^{-kb_2x_3}+A_4e^{kb_2x_3}}{b_3^2-k_1^2\epsilon_1^2b_2^2}\\&-e^{-\frac{b_3}{\epsilon}x_3}\operatorname{cosech}\left(\frac{2b_3}{\epsilon_1}\right)\left(\frac{P_{31}P_3}{b_3^2-k_1^2\epsilon_1^2b_1^2}+\frac{Q_{31}Q_3}{b_3^2-k_1^2\epsilon_1^2b_2^2}\right)\\&+e^{\frac{b_3}{\epsilon}x_3}\operatorname{cosech}\left(\frac{2b_3}{\epsilon_1}\right)\left(\frac{P_{32}P_3}{b_3^2-k_1^2\epsilon_1^2b_1^2}+\frac{Q_{32}Q_3}{b_3^2-k_1^2\epsilon_1^2b_2^2}\right)\Bigg],\end{aligned} \tag{23c}$$

where the auxiliary quantities P_{ij}, Q_{ij} $(i=1,2,3;j=1,2)$ are defined in Appendix D. It is readily verified that the non-local stress components (23) satisfy the natural BCs (5), as a direct consequence of the specific choice of the attenuation functions. Naturally, under the same travelling wave assumption, the non-local stresses (23) may be equally obtained from the differential approach through (4) subject to the boundary conditions (5) and to the extra CBCs (A.8).

At this point, it is fundamental to observe that the CBCs (5) and (A.8) hold by design, i.e. by the very choice of the attenuation functions and irrespectively of the arbitrary constants A_i $(i=1,2,3,4)$. This calls for a deviation from the standard procedure that is followed in classical elasticity, where the BCs set the undetermined constants A_i in the solution. In contrast, in the method of kernel modification, the BCs are fulfilled by the suitable construction of the attenuation functions and therefore the constants A_i are determined by other means, namely by enforcing the equations of motion in the original form (7), prior to the application of the operator $\mathfrak{L}$. Indeed, at this stage, the original motion equations remain unsatisfied and, in fact, they provide precisely the necessary algebraic constraints for the determination of the constants A_i.

Substituting the non-local stress components (23) into the equations of motion (7), one obtains the pair of equations

$$\begin{aligned}&\left(\frac{A_1A_{11}+A_2A_{21}}{b_3^2-k_1^2\epsilon_1^2b_1^2}+\frac{A_3A_{31}+A_4A_{41}}{b_3^2-k_1^2\epsilon_1^2b_2^2}\right)e^{-\frac{b_3x_3}{\epsilon}}\\&+\left(\frac{A_1A_{12}+A_2A_{22}}{b_3^2-k_1^2\epsilon_1^2b_1^2}+\frac{A_3A_{32}+A_4A_{42}}{b_3^2-k_1^2\epsilon_1^2b_2^2}\right)e^{\frac{b_3x_3}{\epsilon}}=0,\end{aligned} \tag{24a}$$

$$\begin{aligned}&\left(\frac{A_1A_{13}+A_2A_{23}}{b_3^2-k_1^2\epsilon_1^2b_1^2}+\frac{A_3A_{33}+A_4A_{43}}{b_3^2-k_1^2\epsilon_1^2b_2^2}\right)e^{-\frac{b_3x_3}{\epsilon}}\\&+\left(\frac{A_1A_{14}+A_2A_{24}}{b_3^2-k_1^2\epsilon_1^2b_1^2}+\frac{A_3A_{34}+A_4A_{44}}{b_3^2-k_1^2\epsilon_1^2b_2^2}\right)e^{\frac{b_3x_3}{\epsilon}}=0,\end{aligned} \tag{24b}$$

that is valid for *any* $x_3\in[-h,h]$. Here, the coefficients $A_{ij},(i,j=1,2,3,4)$ are defined in Appendix D. For these relations to hold at every x_3, the coefficients of the exponential terms must vanish independently and this leads to a homogeneous system of four algebraic linear equations in the four unknown constants A_i $(i=1,2,3,4)$. We now rejoin the standard procedure: A non-trivial solution of this homogeneous system exists if and only if the determinant of the coefficient matrix vanishes, yielding the dispersion equation

$$\det\mathbf{A}=0, \tag{25}$$

where $\mathbf{A}$ is a square matrix of order 4, and $\det\mathbf{A}$ denotes its determinant. As in classical elasticity, this determinant can be factored by the product rule

$$\det\mathbf{A}=-\det\mathbf{A}_s\det\mathbf{A}_o, \tag{26}$$

where

$$\mathbf{A}_s=\begin{bmatrix}A_{11}+A_{12} & A_{31}+A_{32}\\ A_{13}-A_{14} & A_{33}-A_{34}\end{bmatrix},\quad \mathbf{A}_o=\begin{bmatrix}A_{11}-A_{12} & A_{31}-A_{32}\\ A_{13}+A_{14} & A_{33}+A_{34}\end{bmatrix}.$$

This remarkable feature indicates that, similarly to local elasticity, the R-L spectrum decomposes into two distinct spectra, each associated with a specific family of *partial waves*, corresponding to symmetric and anti-symmetric modes, although their identification is not immediately obvious at this stage. Indeed, it should be emphasized that this decomposition property does not immediately follow from the symmetry of the setup as it occurs in local elasticity and it crucially depends on some specific property of the attenuation functions. To further investigate this matter and to reveal the underlying physical nature of these guided modes, in the next Section we develop a systematic decomposition into symmetric and anti-symmetric partial waves.

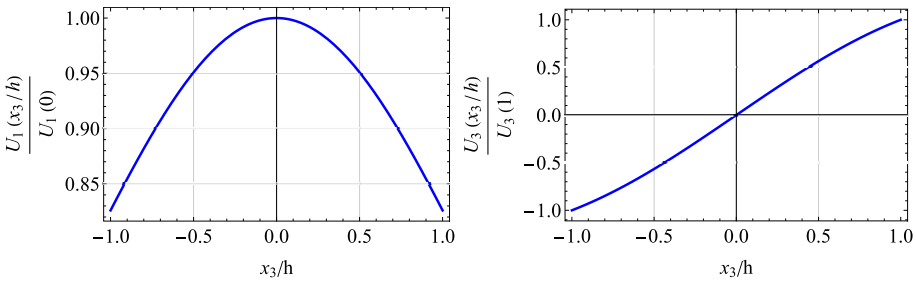

Fig. 1. Longitudinal (left) and transversal (right) normalized displacement components for the symmetric fundamental mode with dimensionless wavenumber $k_1 = 1$ (having let $\kappa = 1.7$ and $\epsilon_1 = 0.15$).

4. Partial waves

As well known from local elasticity, the wave pattern in an elastic strip can be expressed through superposition of symmetric and anti-symmetric (with respect to the mid-plane $x_3 = 0$) partial waves, see Solie and Auld (1973) and Graff (2012). *Symmetric* modes typically govern extensional or breathing-type oscillations; they take the form of longitudinal displacements that are symmetric about the mid-plane of the strip and of transverse displacements that are anti-symmetric. As a result, longitudinal and transversal stresses are even in x_3, while shear stress is odd. In complementary fashion, *anti-symmetric* modes correspond to flexural-type vibrations and exhibit anti-symmetric longitudinal and symmetric transverse displacements. Consequently, longitudinal and transversal stresses are odd in x_3, whereas shear stress is even. Yet, the transposition of these concepts to non-local elasticity is not as straightforward as it may appear at first. Indeed, although displacements can be easily partitioned into symmetric and anti-symmetric modes, the same cannot be immediately said about non-local stresses, whose symmetry properties crucially depend on the properties of the attenuation functions. Consequently, we begin by treating displacements.

4.1. Symmetric waves

Enforcing the afore-mentioned symmetric condition on the displacement field gives

$$u_1(x_1,-x_3,t) = u_1(x_1,x_3,t), \quad u_3(x_1,-x_3,t) = -u_3(x_1,x_3,t), \tag{27}$$

that is most easily expressed in view of the travelling wave assumption as

$$\frac{\mathrm{d}U_1(x_3)}{\mathrm{d}x_3} = 0, \quad U_3(x_3) = 0, \text{ at } x_3 = 0. \tag{28}$$

Plugging this result into the general solution (12), yields the following constraints on the arbitrary constants:

$$A_2 = A_1, \quad A_4 = A_3, \tag{29}$$

whence symmetric modes read

$$\left.\begin{aligned} U_1(x_3) &= 2k^{-1}\left[A_1\cosh\left(kb_1x_3\right) + A_3\cosh\left(kb_2x_3\right)\right], \\ U_3(x_3) &= -2\imath k^{-1}\left[b_1A_1\sinh\left(kb_1x_3\right) + b_2^{-1}A_3\sinh\left(kb_2x_3\right)\right]. \end{aligned}\right\} \tag{30}$$

The normalized amplitudes of the displacement components for symmetric waves corresponding to the fundamental mode with dimensionless wavenumber $k_1 = 1$ are illustrated in Fig. 1. These results parallel those obtained in local elasticity which, in fact, may be retrieved simply by letting

$$b_1 = b_1^{\mathrm{loc}} = \sqrt{1-\frac{v^2}{\kappa^2}}, \quad b_2 = b_2^{\mathrm{loc}} = \sqrt{1-v^2}. \tag{31}$$

The local stresses are immediately obtained from the restricted kinematics (30) and they possess the symmetry property, that is the longitudinal and the transversal local stress (shear stress) are even (odd) with respect to x_3. Conversely, in general, the non-local stress is not guaranteed to satisfy the same symmetry property as the local stress from which it is obtained. Indeed, for this to happen, the kernel function must satisfy the mirror symmetry property (21), which guarantees that the symmetry property of the local stress translates into an equivalent property for the non-local stress. This statement is proved in Appendix B. To confirm this result, non-local stresses are presented in Fig. 2 and they clearly satisfy the same symmetry property as the local stresses, namely

$$\frac{\mathrm{d}T_{11}^{\mathrm{sym}}(x_3)}{\mathrm{d}x_3} = \frac{\mathrm{d}T_{33}^{\mathrm{sym}}(x_3)}{\mathrm{d}x_3} = T_{13}^{\mathrm{sym}}(x_3) = 0, \quad \text{at } x_3 = 0. \tag{32}$$

Together, conditions (28) and (32) correspond to Mindlin-type mid-plane boundary conditions (Mindlin, 1960), see Fig. 3 and cfr. Nobili et al. (2020) for the same concepts applied to strain gradient theories. Such conditions, therefore, hold in non-local elasticity *provided that mirror-symmetry holds for the kernel functions* (specifically across x_3).

Mindlin mid-plane conditions may be used to deduce a new pair of attenuation functions, $G_s(\boldsymbol{x},\boldsymbol{\xi})$ and $G_o(\boldsymbol{x},\boldsymbol{\xi})$, which are given in Appendix B. Specifically, G_s is used in association with the even transversal stress to give

$$T_{33}^{\mathrm{sym}}(x_3)e^{\imath kx_1} = 2\int_{-\infty}^{\infty}\mathrm{d}\xi_1\int_0^h G_s(x_1,x_3,\xi_1,\xi_3)S_{33}(\xi_3)e^{\imath k\xi_1}\mathrm{d}\xi_3,$$

while G_o operates on the odd local shear stress to give

$$T_{13}^{\mathrm{sym}}(x_3)e^{\imath kx_1} = 2\int_{-\infty}^{\infty}\mathrm{d}\xi_1\int_0^h G_o(x_1,x_3,\xi_1,\xi_3)S_{13}(\xi_3)e^{\imath k\xi_1}\mathrm{d}\xi_3.$$

It is easy to see that the corresponding non-local stresses correspond to those derived with the use of the general kernels (18) and (A.2). Indeed, mirror symmetry across x_3 allows to obtain the connection (we omit x_1 and ξ_1 here to lighten notation)

$$G_{s,o}(x_3,\xi_3) = \begin{cases} \frac{1}{2}\left[f_1(x_3,\xi_3) \pm f_1(x_3,-\xi_3)\right], & x_3 > \xi_3 > 0, \\ \frac{1}{2}\left[f_2(x_3,\xi_3) \pm f_2(-\xi_3,x_3)\right], & \xi_3 > x_3 > 0, \end{cases} \tag{33}$$

where

$$G_2(x_3,\xi_3) = \begin{cases} f_1(x_3,\xi_3), & x_3 > \xi_3 > 0 \\ f_2(x_3,\xi_3), & \xi_3 > x_3 > 0 \end{cases}. \tag{34}$$

This result, that is proved in Appendix B, allows to decompose the kernel G_2 into its symmetric/anti-symmetric components, which may be used to study partial waves. Compared to the procedure presented in Section 3, the partial wave approach appears simpler and more physically informative. Tangentially, it is observed that the kernel G_1, being of the difference type, coincides with its symmetric and anti-symmetric components and therefore demands no decomposition.

By using the constraints (29) on the arbitrary constants A_i, we deduce that the non-local stress components (23) satisfy the equations of motion (7) (the same result can be immediately derived from Eq. (24)) if

$$\frac{A_{11}+A_{12}}{b_3^2-k_1^2\epsilon_1^2b_1^2}A_1 + \frac{A_{31}+A_{32}}{b_3^2-k_1^2\epsilon_1^2b_2^2}A_3 = 0, \tag{35a}$$

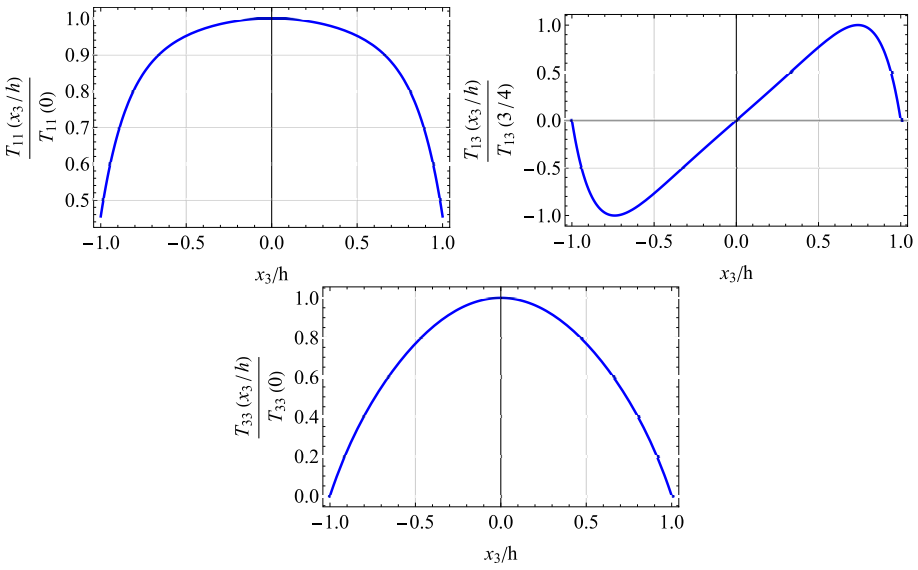

Fig. 2. Longitudinal (top-left), shear (top-right), and transversal (bottom) non-local normalized stress components for the symmetric fundamental mode with dimensionless wavenumber $k_1 = 1$ (having let $\kappa = 1.7$ and $\epsilon_1 = 0.15$).

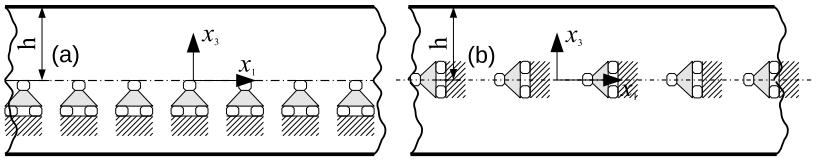

Fig. 3. Mindlin mid-plane conditions for symmetric (a) and anti-symmetric (b) modes.

$$\frac{A_{13}-A_{14}}{b_3^2-k_1^2\epsilon_1^2b_1^2}A_1+\frac{A_{33}-A_{34}}{b_3^2-k_1^2\epsilon_1^2b_2^2}A_3=0, \tag{35b}$$

that is a homogeneous linear system in A_1, A_3. For non-trivial solutions to exist, the determinant of the coefficient matrix must vanish, which fact yields the dispersion relation

$$D_s=\det\mathbf{A}_s=0, \tag{36}$$

which corresponds to the first factor in the decomposition (26). Explicitly, the dispersion relation (36) reads

$$\left[P_2Q_3\mathcal{T}_1-P_3Q_2\mathcal{T}_2\right]\left[1+\tanh\left(\epsilon_1^{-1}b_3\right)\right]+\epsilon_1D_{s1}+\epsilon_1^2D_{s2}+\epsilon_1^3D_{s3}=0, \tag{37}$$

where we have let the shorthands ($\mathcal{T}_1=\tanh\left(k_1b_1\right)$, $\mathcal{T}_2=\tanh\left(k_1b_2\right)$)

$$\begin{aligned}
D_{s1}&=-k_1b_3^{-1}\left(P_3Q_1-P_1Q_3\right)\tanh\left(\epsilon_1^{-1}b_3\right),\\
D_{s2}&=k_1^2b_3^{-2}\left\{\left[P_2Q_1\mathcal{T}_1-P_1Q_2\mathcal{T}_2\right]+\left[b_1P_1Q_3\mathcal{T}_1-b_2P_3Q_1\mathcal{T}_2\right]\tanh\left(\epsilon_1^{-1}b_3\right)\right\},\\
D_{s3}&=k_1^3b_3^{-3}\left(b_2P_2Q_1-b_1P_1Q_2\right)\mathcal{T}_1\mathcal{T}_2,
\end{aligned}$$

and P_i and $Q_i, i\in\{1,2,3\}$, are defined in Eqs. (16). Yet, for small values of the non-local parameter ϵ_1, we can expand this involved dispersion relation as

$$4b_2^{\mathrm{loc}}b_1^{\mathrm{loc}}\tanh\left(k_1b_1^{\mathrm{loc}}\right)-\left(2-v^2\right)^2\tanh\left(k_1b_2^{\mathrm{loc}}\right)=O(\varepsilon_1), \tag{38}$$

that recovers the classical Rayleigh–Lamb dispersion relation for symmetric modes in local elasticity, originally derived by Lamb (1917, Eq.(12)).

4.2. Anti-symmetric waves

For anti-symmetric waves the conditions on displacement fields are

$$u_1(x_1,-x_3,t)=-u_1(x_1,x_3,t),\quad u_3(x_1,-x_3,t)=u_3(x_1,x_3,t), \tag{39}$$

and, in view of the travelling wave assumption (10), the conditions at the mid-plane become

$$U_1(x_3)=0,\quad \frac{\mathrm{d}U_3(x_3)}{\mathrm{d}x_3}=0,\ \text{at } x_3=0. \tag{40}$$

Following the general solution of the displacement amplitude (12), this yields the constraints

$$A_2=-A_1,\quad A_4=-A_3, \tag{41}$$

which provide the displacement for anti-symmetric modes

$$\left.\begin{aligned}
U_1(x_3)&=-2k^{-1}\left[A_1\sinh\left(kb_1x_3\right)+A_3\sinh\left(kb_2x_3\right)\right],\\
U_3(x_3)&=2\imath k^{-1}\left[b_1A_1\cosh\left(kb_1x_3\right)+\tfrac{A_3}{b_2}\cosh\left(kb_2x_3\right)\right].
\end{aligned}\right\} \tag{42}$$

These are represented in Fig. 4 for the fundamental mode $k_1 = 1$. In this case, the longitudinal displacement exhibits anti-symmetry about the mid-plane, while the transverse motion is symmetric. It follows that longitudinal and transversal local stresses are now anti-symmetric, while shear stress is symmetric. On account of the mirror property of the kernels, such behaviour is reproduced by the non-local stresses that are shown in Fig. 5. The same results are obtained via the symmetric kernel G_s

$$T_{13}^{\mathrm{skw}}(x_3)e^{\imath kx_1}=2\int_{-\infty}^{\infty}\mathrm{d}\xi_1\int_0^h G_s(x_1,x_3,\xi_1,\xi_3)S_{13}^{\mathrm{skw}}(\xi_3)e^{\imath k\xi_1}\mathrm{d}\xi_3,$$

and the anti-symmetric kernel G_o

$$T_{33}^{\mathrm{skw}}(x_3)e^{\imath kx_1}=2\int_{-\infty}^{\infty}\mathrm{d}\xi_1\int_0^h G_o(x_1,x_3,\xi_1,\xi_3)S_{33}^{\mathrm{skw}}(\xi_3)e^{\imath k(\xi_1-vt)}\mathrm{d}\xi_3.$$

Mindlin mid-plane boundary conditions read

$$U_1(x_3)=0,\quad T_{33}^{\mathrm{skw}}(x_3)=0,\ \text{at } x_3=0, \tag{43}$$

and they are represented in Fig. 3b.

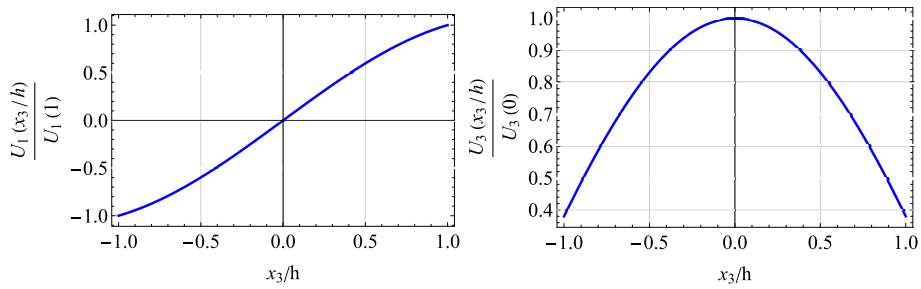

Fig. 4. Longitudinal (left) and transversal (right) normalized displacement components for the fundamental anti-symmetric mode with dimensionless wavenumber $k_1 = 1$ (having let $\kappa = 1.7$ and $\epsilon_1 = 0.15$).

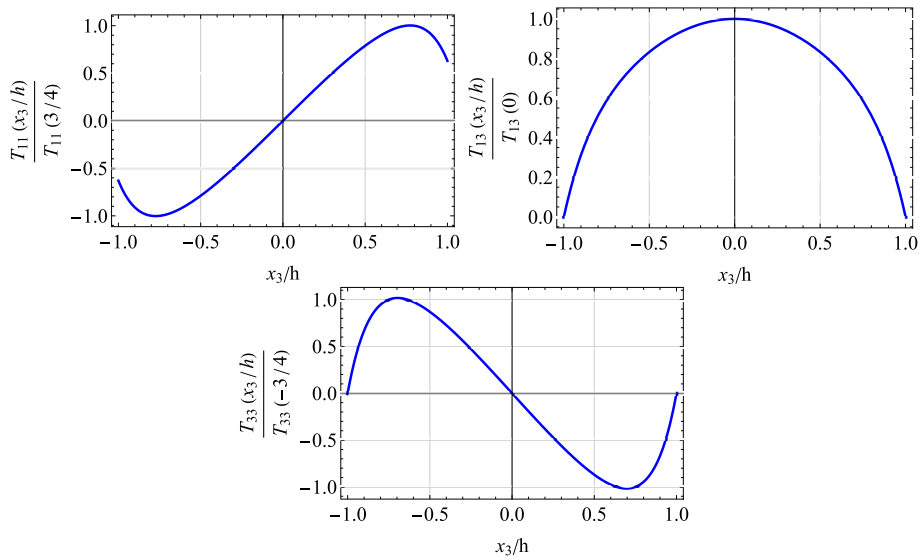

Fig. 5. Longitudinal (top-left), shear (top-right), and transversal (bottom) non-local normalized stress components for the fundamental anti-symmetric mode with dimensionless wavenumber $k_1 = 1$ (having let $\kappa = 1.7$ and $\epsilon_1 = 0.15$).

Thus, in light of Eqs. (41), the non-local stress components (23) satisfy the equations of motion (7) (equivalently one may use Eq. (24)) when

$$\frac{A_{11} - A_{12}}{b_3^2 - k_1^2\epsilon_1^2 b_1^2} A_1 + \frac{A_{31} - A_{32}}{b_3^2 - k_1^2\epsilon_1^2 b_2^2} A_3 = 0, \tag{44a}$$

$$\frac{A_{13} + A_{14}}{b_3^2 - k_1^2\epsilon_1^2 b_1^2} A_1 + \frac{A_{33} + A_{34}}{b_3^2 - k_1^2\epsilon_1^2 b_2^2} A_3 = 0, \tag{44b}$$

that lends a homogeneous system of linear equations in A_1 and A_3. For a non-trivial solution to exist, the determinant of the coefficient matrix must vanish

$$D_o = \det \mathbf{A}_o = 0, \tag{45}$$

which corresponds to the second factor in the decomposition (26). Explicitly, we get the dispersion equation ($\mathcal{T}_1 = \tanh(k_1 b_1)$, $\mathcal{T}_2 = \tanh(k_1 b_2)$)

$$\left[P_2 Q_3 \mathcal{T}_2 - P_3 Q_2 \mathcal{T}_1\right]\left[1 + \tanh\left(\epsilon_1^{-1} b_3\right)\right] + \epsilon_1 D_{o1} + \epsilon_1^2 D_{o2} + \epsilon_1^3 D_{o3} = 0, \tag{46}$$

where

$$D_{o1} = -k_1 b_3^{-1}\left(P_3 Q_1 - P_1 Q_3\right)\mathcal{T}_1\mathcal{T}_2,$$
$$D_{o2} = k_1^2 b_3^{-2}\left\{\left[b_1 P_1 Q_3 \mathcal{T}_2 - b_2 P_3 Q_1 \mathcal{T}_1\right] + \tanh\left(\epsilon_1^{-1} b_3\right)\left[P_2 Q_1 \mathcal{T}_2 - P_1 Q_2 \mathcal{T}_1\right]\right\},$$
$$D_{o3} = k_1^3 b_3^{-3}\left(b_2 P_2 Q_1 - b_1 P_1 Q_2\right)\tanh\left(\epsilon_1^{-1} b_3\right).$$

For small values of the non-local parameter ϵ_1, this gives

$$4 b_2^{\mathrm{loc}} b_1^{\mathrm{loc}} \tanh\left(k_1 b_2^{\mathrm{loc}}\right) - \left(2 - \upsilon^2\right)^2 \tanh\left(k_1 b_1^{\mathrm{loc}}\right) = O(\epsilon_1), \tag{47}$$

that corresponds to the well-known expression originally derived by Lamb (1917, Eq.(48)) for anti-symmetric Rayleigh–Lamb modes in local elasticity. Appendix C shows that enforcing zero *non-local* stress does not entail that the corresponding *local* stress also disappears, a ill-conceived presumption that often appears in the literature.

5. Dispersion analysis

In this Section, the dispersion relations derived for symmetric (36) and anti-symmetric (45) modes are explored numerically to highlight the effect of non-locality on the propagation characteristics. Specifically, we are interested in deviations from the classical R-L spectrum and in their significance with respect to the intrinsic length scale.

Fig. 6 plots the fundamental dispersion branches for symmetric and for anti-symmetric R-L modes (solid) and compares them with the relevant branches obtained within local elasticity (dotted). The incorporation of non-locality, governed by the intrinsic material length scale ϵ_1, produces a clear deviation from the classical behaviour. Specifically, in the long-wavelength limit $k_1 \to 0$, the non-local and the local dispersion curves for the fundamental *anti-symmetric* mode coincide, although the slope is clearly different. Conversely, the corresponding curves for the fundamental *symmetric* mode depart significantly and

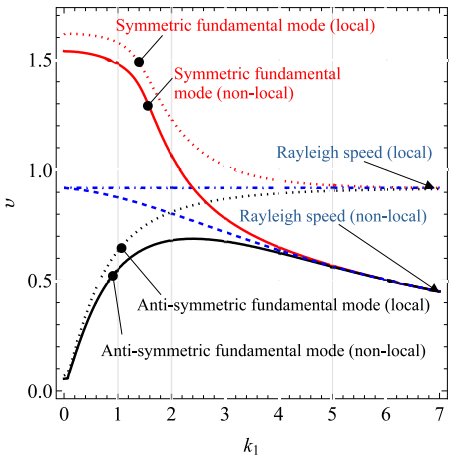

Fig. 6. Non-local dispersion curve (solid) for the fundamental symmetric (red) and anti-symmetric (black) R-L mode, compared with the corresponding classical branches of local elasticity (dotted, red for symmetric and black for anti-symmetric). As expected and for both local and non-local elasticity, fundamental modes asymptote to the Rayleigh surface wave speed which, however, is constant in local elasticity (blue-dot-dashed) and monotonically decreases in non-local elasticity (blue-dashed). Here, $\epsilon_1 = 0.2$, $\kappa = 1.7$. (For interpretation of the references to colour in this figure legend, the reader is referred to the web version of this article.)

indeed the relevant cut-off velocities are different. These deviations are very significant for reduced dimensional models (Nobili, 2021) and a possible mechanical explanation is herein given. Looking at the other end of the spectrum, as $k_1 \gg 1$ corresponding to short wavelengths, it is well-known that the fundamental modes asymptote to the Rayleigh wave speed and this is indeed the case shown in Fig. 6, bearing in mind that, unlike local elasticity, the Rayleigh speed in the non-local theory is dispersive, see Nobili and Pramanik (2025a, Eq.(29)). In contrast, higher modes, either symmetric or skew-symmetric, asymptote to either of the bulk wave speeds υ_S and υ_L, as it clearly appears looking at Figs. 7 and 8 which plot symmetric and anti-symmetric modes, respectively. Therefore, it may be argued that the fundamental modes are connected to a localized behaviour that is very sensitive to the presence of the boundaries; their deviation from the classical spectrum is essentially a result of the presence of the surface of the medium, that is accounted for via kernel modification. Indeed, this effect is especially relevant for symmetric modes, that may run parallel to the surface, and much less so for anti-symmetric modes, in view of the symmetric layout (of the boundaries).

Figs. 7 and 8 describe the influence of the non-local parameter ϵ_1 on the dispersion of symmetric and anti-symmetric modes. Clearly, the entire R-L spectrum can be parted into three separate regions in the $(k_1 - \upsilon)$ plane, according to the real or imaginary nature of the attenuation indices b_1 and b_2. The first region (R-I) corresponds to b_1 and b_2 both real: these are evanescent modes along the thickness and, as anticipated, they run parallel to the surfaces, with phase velocity in the range $\upsilon < \upsilon_S$. The second region (R-II) is characterized by b_1 real and b_2 imaginary, whence one wave is still travelling (yet with phase velocity $\upsilon_S < \upsilon < \upsilon_L$), while the other propagates along the thickness and therefore bounces off the surfaces. Finally, in the third region (R-III), both b_1 and b_2 are imaginary and both waves propagate along the thickness, although they also travel in the longitudinal direction with ultra-sonic speed $\upsilon < \upsilon_L$. As in local elasticity, Figs. 7 and 8 show that the regions R-II and R-III accommodate two distinct families of higher modes which asymptote the non-local shear or longitudinal bulk wave velocity, respectively, whereas the region R-I only contains the fundamental symmetric and anti-symmetric modes, which, as previously anticipated when discussing Fig. 6, converge to the Rayleigh wave speed. As the non-local parameter ϵ_1 increases, higher modes located in the regions R-II and R-III progressively cluster together and collapse onto the relevant non-local body wave limit. Besides, the larger ϵ_1, the sooner this collapse takes place in terms of wavenumber, indicating that non-locality becomes relevant at shorter and shorter wavelengths.

To further illustrate the collapse of higher modes discussed above, Fig. 9 presents the influence of the non-local parameter ϵ_1 on both symmetric and anti-symmetric waves. It is observed that, as ϵ_1 increases, dispersion curves systematically move down, at lower phase speed υ, thus reflecting the softening effect induced by non-locality. More specifically, this softening effect is more pronounced for short wavelengths, given that such modes are more sensitive to the microstructural features associated with the internal length scale.

Fig. 10 illustrates the dispersion behaviour of both symmetric and anti-symmetric R-L modes at different values of ratio κ. An increase in κ equates to a bigger value of the Poisson's ratio ν through the relation $\kappa = \sqrt{2(1-\nu)/(1-2\nu)}$. The influence of κ on higher-order modes (beyond the fundamental modes) can be appreciated dividing the dispersion plane into two sectors: the lower (upper) sector, defined by $\upsilon \lessgtr \upsilon_{\text{Lamé}} \equiv \sqrt{2}/b_3$, denoted as sector S-I (S-II). The intersection of the curve $\upsilon = \upsilon_{\text{Lamé}}$ with the R-L branches defines the non-local Lamé curve, obtained from the special condition $b_2 = \imath$ (Graff, 2012, §8.1.5), which is independent of κ and yet dependent on the wavenumber k_1 through the non-local parameter ϵ_1.

It is observed that, as κ increases, the phase velocity of the modes in sector S-II grows, sometimes by a large amount, whereas the dispersion curves in sector S-I remain almost unaffected. Consequently, inside sector S-I, the role of κ or ν on the R-L dispersion pattern is greatly reduced. However, this observation does not hold for the fundamental modes that move upwards towards larger wave speeds υ whenever κ increases, although this movement is less pronounced compared to that of the higher modes in sector S-II. Interestingly, larger values of κ are associated with higher cut-off phase speeds for the fundamental symmetric mode, as a consequence of the transition of the dispersion curve from flat (near the cut-off) to vertical being smeared out. A similar weak dependence of dispersion branches on the bulk wave velocity ratio κ (or, equivalently, on Poisson's ratio ν) in the low-velocity region (S-I) has also been reported in earlier studies (see Ryden et al. (2003), Fig. 6b; and Royer et al. (2009), Figs. 1-2).

6. Conclusions

In this paper we have studied R-L guided waves in an elastic isotropic strip within the framework of non-local elasticity. Since the governing equations of the non-local theory are generally over-determined due to the presence of implicit constitutive boundary conditions (CBCs) embedded in the attenuation functions, a kernel modification procedure is employed. This approach, previously introduced by the authors for 1D (Nobili and Pramanik, 2025b; Pramanik and Nobili, 2025) and 2D (Nobili and Pramanik, 2025a) non-local problems, modifies the Green's function kernel so that the resulting CBCs coincide with the natural boundary conditions (BCs), while preserving kernel symmetry and the quadratic nature of the strain energy density. Once the formulation is made well-posed, the problem is solved, under the usual travelling wave assumption, through the integral formulation and the corresponding non-local stresses are determined in closed form. These depend on four unknown constants whose determination calls for the equations of motion. Indeed, unlike local elasticity, the (non-local) stresses already satisfy the natural BCs of the problem, which were used for the construction of the attenuation functions. Thus, the equations of motion lend to a linear homogeneous system of equations whose determinant set the dispersion relation for R-L waves. Similarly to local elasticity, this dispersion equation naturally decomposes into symmetric and anti-symmetric components, although this feature is here not obvious and depends on some symmetry property embedded in the kernel functions. The identification of this property allows to decompose the attenuation functions in their symmetric and

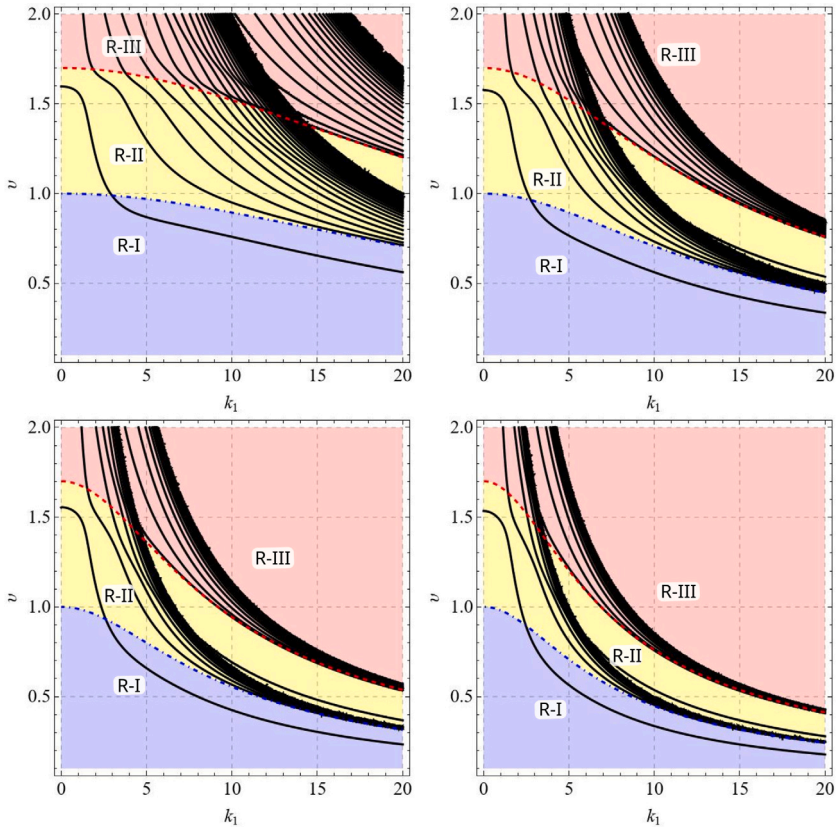

Fig. 7. Dispersion curves (black, solid) for symmetric R-L waves for different values of the non-local parameter: $\epsilon_1 = 0.05$ (top, left), $\epsilon_1 = 0.10$ (top, right), $\epsilon_1 = 0.15$ (bottom, left), and $\epsilon_1 = 0.20$ (bottom, right) with body wave velocity ratio $\kappa = 1.7$. Two asymptotic curves, corresponding to $\upsilon = \upsilon_L$ (red, dashed) and $\upsilon = \upsilon_S$ (blue, dot-dashed).

anti-symmetric parts, which may be used to solve the corresponding dispersion problem independently, with a significant reduction in complexity. Indeed, we may argue that this symmetry property should be listed among the classical unity, reciprocity and impulsivity properties which are demanded in the literature for any meaningful attenuation function.

Results show that the fundamental symmetric and anti-symmetric modes asymptote to the Rayleigh surface wave velocity for large wavenumbers, whereas the higher modes form two distinct groups that approach the corresponding non-local bulk wave velocities. This confirms the physical consistency of the non-local formulation. The presence of the intrinsic length-scale parameter, however, clearly produces size-dependent effects, which are especially relevant at short wavelengths. As expected, these effects are most pronounced for the higher modes, which exhibit greater phase-velocity reduction and reduced modal spacing. Yet, an important deviation from the local theory is also demonstrated for the fundamental modes, which has strong bearing on the underlying beam theory. The effect of the bulk wave velocity ratio κ is also examined: Increasing κ (or, equivalently, the Poisson's ratio) enhances the phase velocity primarily in the higher modes of the upper sector (S-II), where the wavespeed exceeds that of the Lamé mode, while producing negligible influence in the lower sector (S-I). This behaviour reflects a weak dependence of dispersion characteristics on the Poisson's ratio in certain velocity regimes, consistent with previous observations in isotropic plate (local) theories.

Overall, this work establishes a well-posed non-local elasticity framework capable of accurately capturing microstructure-dependent dispersion behaviour in guided waves. The presented formulation not only generalizes the classical R-L theory but also opens new perspectives for interpreting ultrasonic wave propagation in thin films, nano-layered composites, architected materials and every time size-dependent effects are non-negligible.

CRediT authorship contribution statement

Dipendu Pramanik: Writing – original draft, Investigation, Formal analysis, Conceptualization. **Andrea Nobili:** Writing – review & editing, Writing – original draft, Supervision, Investigation, Funding acquisition, Formal analysis, Conceptualization. **Santanu Manna:** Writing – review & editing.

Declaration of competing interest

The authors declare the following financial interests/personal relationships which may be considered as potential competing interests: Andrea Nobili reports financial support was provided by European Union. If there are other authors, they declare that they have no known competing financial interests or personal relationships that could have appeared to influence the work reported in this paper.

Acknowledgements

We acknowledge financial support under the National Recovery and Resilience Plan (NRRP), Mission 4, Component 2, Investment 1.1, Call for tender No. 1409 published on 14.9.2022 by the Italian Ministry of University and Research (MUR), funded by the European Union NextGenerationEU, Project Title: Sustainable CompositE materials for the construction iNdusTry - CUP P2022P3Y2T - Grant Assignment Decree No. 1381 adopted on 1.9.2023 by the Italian Ministry of University and Research (MUR). AN is grateful for the support of the National

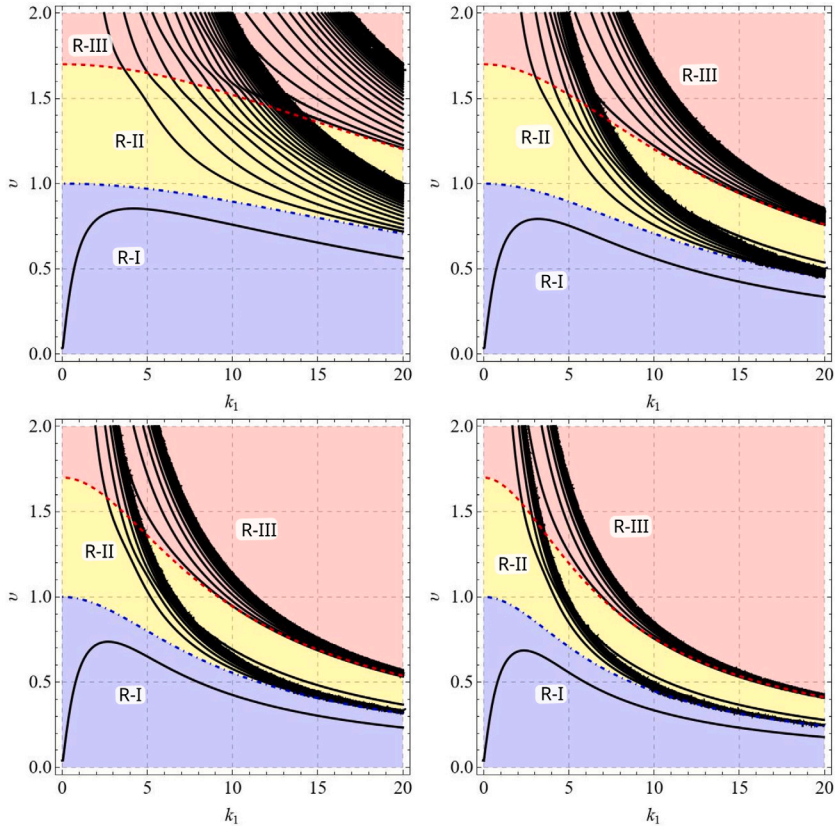

Fig. 8. Dispersion curves (black, solid) for anti-symmetric R-L waves for different non-local parameter: $\epsilon_1 = 0.05$ (top, left), $\epsilon_1 = 0.10$ (top, right), $\epsilon_1 = 0.15$ (bottom, left), and $\epsilon_1 = 0.20$ (bottom, right) with body wave velocity ratio $\kappa = 1.7$. Two asymptotic curves, corresponding to $v = v_S$ (red, dashed) and $v = v_L$ (blue, dot-dashed).

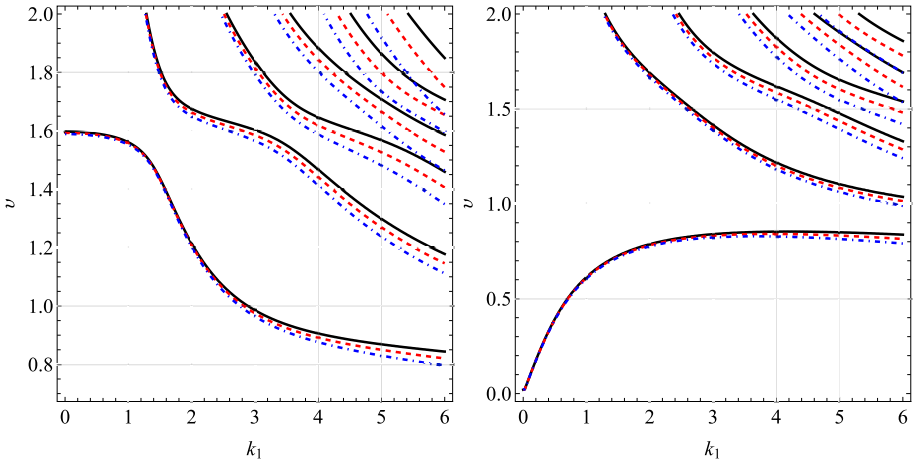

Fig. 9. Dispersion curves for symmetric (left) and anti-symmetric (right) R-L waves for different non-local parameter: $\epsilon_1 = 0.05$ (black,solid), $\epsilon_1 = 0.06$ (red, dashed), and $\epsilon_1 = 0.07$ (blue, dot-dashed), with body wave velocity ratio $\kappa = 1.7$.

Group of Mathematical Physics (GNFM), a group of the Italian Institute of Higher Mathematics (INdAM).

Appendix A. Attenuation functions and corresponding CBCs

In this section, we discuss the construction of the attenuation functions for the non-local differential operator $\mathfrak{L} \equiv 1 - \epsilon^2 \nabla^2$ and derive the associated constitutive boundary conditions (CBCs) that naturally emerge from the kernel representation. This analysis provides a rigorous basis for the boundary operators that must accompany the differential form of Eringen's non-local elasticity.

The Green's function of $\mathfrak{L}$ in the two-dimensional infinite plane is well known to be

$$G_1(x_1, x_3; \xi_1, \xi_3) = \frac{1}{2\pi\epsilon^2} K_0\left(\epsilon^{-1}\sqrt{(x_1-\xi_1)^2 + (x_3-\xi_3)^2}\right). \tag{A.1}$$

where $K_0(\cdot)$ denotes the modified Bessel function of the second kind of order zero. The kernel $G_1(x_1, x_3; \xi_1, \xi_3)$ is the fundamental non-local modulus introduced by Eringen (1983). It plays the role of a non-local

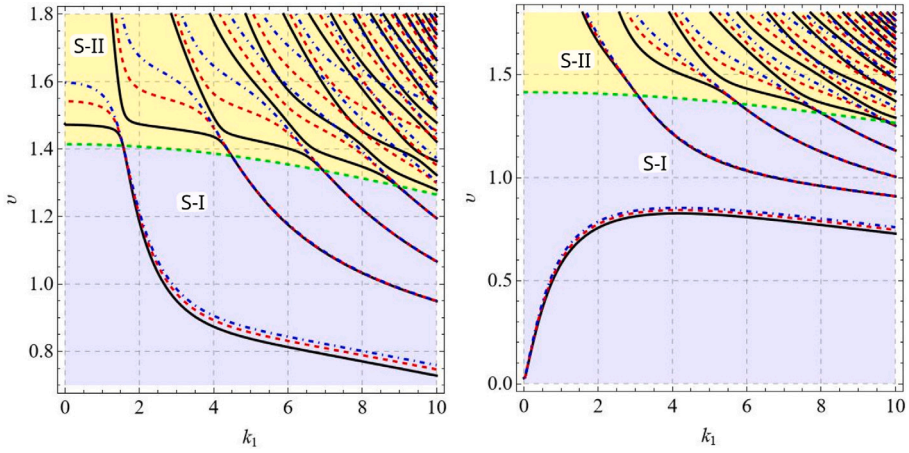

Fig. 10. Dispersion curves for symmetric (left) and anti-symmetric (right) R-L waves for different ratios of bulk wave speed: $\kappa = 1.5$ (black,solid), $\kappa = 1.6$ (red, dashed), and $\kappa = 1.7$ (blue, dot-dashed), having let $\epsilon_1 = 0.05$. The non-local Lamé curve is also shown (green-dashed), which collects particular points in the Rayleigh–Lamb spectrum that are independent of κ and for which $b_2 = \imath$. (For interpretation of the references to colour in this figure legend, the reader is referred to the web version of this article.)

kernel, weighting the contribution of the classical stress field σ at point (ξ_1, ξ_3) to the non-local stress T at (x_1, x_3).

An equivalent Fourier representation of (A.1), obtained via standard transform identities (Nobili and Pramanik, 2025a), is

$$G_1(x_1, x_3; \xi_1, \xi_3) = \frac{1}{4\pi^2\epsilon^2} \iint_{-\infty}^{\infty} \frac{\exp\left\{-\imath\left[\eta_1\epsilon^{-1}(x_1-\xi_1) + \eta_3\epsilon^{-1}(x_3-\xi_3)\right]\right\}}{1+\eta_1^2+\eta_3^2} \mathrm{d}\eta_1 \mathrm{d}\eta_3, \tag{A.2}$$

where η_1 and η_3 denote the Fourier (spectral) variables conjugate to the spatial coordinates x_1 and x_3, respectively. This is particularly useful for deriving constitutive boundary conditions. Indeed, for any non-local stress t_{ij} that it is associated with the kernel G_1, we can omit the time-harmonic factor (since it plays no role in the derivation of the CBCs) and introduce the reduced spatial stress field

$$T(x_1, x_3) = \int_{-h}^{h} \mathrm{d}\xi_3 \int_{-\infty}^{\infty} G_1(x_1, x_3; \xi_1, \xi_3)\, \sigma(\xi_1, \xi_3)\, \mathrm{d}\xi_1. \tag{A.3}$$

Substituting the Fourier representation (A.2) for G_1 and interchanging the order of integration yields

$$T(x_1, x_3) = \frac{1}{4\pi^2\epsilon^2} \int_{-h}^{h}\mathrm{d}\xi_3 \int_{-\infty}^{\infty}\mathrm{d}\xi_1 \int_{-\infty}^{\infty}\mathrm{d}\eta_3 \int_{-\infty}^{\infty} \frac{e^{-\imath\left[\eta_1\epsilon^{-1}(x_1-\xi_1)+\eta_3\epsilon^{-1}(x_3-\xi_3)\right]}}{1+\eta_1^2+\eta_3^2} \sigma(\xi_1, \xi_3)\mathrm{d}\eta_1. \tag{A.4}$$

Taking a linear combination and performing the integration with respect to η_1, one gets

$$\frac{\partial T(x_1, x_3)}{\partial x_3} + \alpha\, T(x_1, x_3) = \frac{1}{4\pi\epsilon^2} \int_{-h}^{h}\mathrm{d}\xi_3 \int_{-\infty}^{\infty}\mathrm{d}\eta_3 \int_{-\infty}^{\infty} \frac{\alpha - \imath\epsilon^{-1}\eta_3}{\sqrt{1+\eta_3^2}} e^{-\epsilon^{-1}|x_1-\xi_1|\sqrt{1+\eta_3^2} - \imath\eta_3\epsilon^{-1}(x_3-\xi_3)} \sigma(\xi_1, \xi_3)\mathrm{d}\xi_1, \tag{A.5}$$

where α is a free constant that is determined by enforcing vanishing boundary contributions.

For harmonic plane waves propagating in the x_1-direction with wavenumber k, we have $\sigma(x_1, x_3) = S(x_3)e^{\imath k x_1}$. Carrying out the integration with respect to ξ_1 and simplifying, Eq. (A.5) reduces to

$$\frac{\partial T(x_1, x_3)}{\partial x_3} + \alpha\, T(x_1, x_3) = \frac{1}{2\pi\epsilon} e^{\imath k x_1} \int_{-h}^{h}\mathrm{d}\xi_3 \int_{-\infty}^{\infty} \frac{\alpha - \imath\epsilon^{-1}\eta_3}{b_3^2+\eta_3^2} \exp\left[-\imath\eta_3\epsilon^{-1}(x_3-\xi_3)\right] S(\xi_3)\mathrm{d}\eta_3, \tag{A.6}$$

and performing the integration with respect to η_3 via the residue method (we close the integration path in the upper/lower half-complex plane when $x_3 \lessgtr \xi_3$) finally gives

$$\frac{\partial T(x_1, x_3)}{\partial x_3} + \alpha\, T(x_1, x_3) = \frac{1}{2\epsilon b_3} e^{\imath k x_1} \int_{-h}^{h} \left(\alpha - \mathrm{sgn}(x_3-\xi_3)\epsilon^{-1}b_3\right) \exp\left[-\epsilon^{-1}|x_3-\xi_3|b_3\right] S(\xi_3)\mathrm{d}\xi_3, \tag{A.7}$$

where $\mathrm{sgn}(x) = 2H(x) - 1$ denotes the *sign function* and $H(x)$ is Heaviside's function. Thus, at the boundary $x_3 = \pm h$, the above integral trivially evaluates to zero for $\alpha = \pm\epsilon^{-1}b_3$. This implies that the CBC for the case of harmonic plane waves with wavenumber k and for the Green's function G_1, are given by

$$\frac{\partial T(x_1, x_3)}{\partial x_3} \pm \epsilon^{-1} b_3\, T(x_1, x_3) = 0, \text{ at } x_3 = \pm h. \tag{A.8}$$

We now aim to construct the non-local kernel (Green's function or non-local modulus) for which the associated non-local stress components vanish at the strip boundaries $x_3 = \pm h$. In other words, we seek a Green's function G_2 for the non-local operator $\mathfrak{L}$ in the finite strip $\mathbb{V}$, such that

$$\mathfrak{L}G_2(x_1, x_3; \xi_1, \xi_3) = \delta(x_1-\xi_1)\delta(x_3-\xi_3), \quad -h \le x_3 \le h, \tag{A.9}$$

subject to the homogeneous Dirichlet boundary conditions

$$G_2(x_1, \pm h; \xi_1, \xi_3) = 0. \tag{A.10}$$

A convenient way to solve this problem is to apply the Fourier transform in the unbounded x_1-direction according to

$$\overline{G_2}(s; x_3, \xi_3) = \int_{-\infty}^{\infty} G_2(x_1, x_3; \xi_1, \xi_3) e^{\imath s(x_1-\xi_1)} \mathrm{d}x_1, \tag{A.11}$$

where the definition is slightly modified from the usual to avoid expressing the term $e^{-\imath s\xi_1}$ throughout the Fourier transforms. This reduces the governing Eq. (A.9) to the inhomogeneous ODE

$$\left(-\frac{\mathrm{d}^2}{\mathrm{d}x_3^2} + \beta^2\right) \overline{G_2}(s; x_3, \xi_3) = \epsilon^{-2}\delta(x_3-\xi_3), \tag{A.12}$$

where $\beta = \epsilon^{-1}\sqrt{1+s^2\epsilon^2}$. Solving the latter by imposing the continuity condition at $x_3 = \xi_3$ together with the jump condition in derivative coming from the delta function, as well as the boundary conditions (A.10), one obtains

$$\overline{G_2}(s; x_3, \xi_3) = \frac{\cosh\left\{\beta\left(2h - |x_3-\xi_3|\right)\right\} - \cosh\left\{\beta\left(x_3+\xi_3\right)\right\}}{2\epsilon^2\beta\sinh(2\beta h)}, \tag{A.13}$$

The full Green's function in physical space is then obtained by the inverse Fourier transform,

$$G_2(x_1,x_3;\xi_1,\xi_3)=\frac{1}{2\pi}\int_{-\infty}^{\infty}\overline{G_2}(s;x_3,\xi_3)e^{-\imath s(x_1-\xi_1)}\mathrm{d}s. \tag{A.14}$$

An alternative but equivalent construction is based on the *image method*, as the Green's function G_1 for the operator $\mathfrak{L}$ in the unbounded plane is already known [cf. Eq. (A.1)]. Following the classical construction (see Melnikov and Melnikov (2012)), the method proceeds by placing successive image sources and sinks symmetrically outside the strip. Specifically, for a original source at (ξ_1,ξ_3), we introduce unit sinks at $(\xi_1,-\xi_3+(4m+2)h)$ and unit sources at (ξ_1,ξ_3+4mh), for all integer $m\in\mathbb{Z}$. These image points are distributed periodically above and below the strip, reflected about the planes $x_3=\pm h$. The contributions of the image system at the field point (x_1,x_3) are given by $-G_1(x_1,x_3;\xi_1,-\xi_3+(4m+2)h)$ for the sinks and $G_1(x_1,x_3;\xi_1,\xi_3+4mh)$ for the sources.

Summing over the infinite sequence of sources and sinks, the resulting Green's function is expressed as

$$\begin{aligned}&G_2(x_1,x_3;\xi_1,\xi_3)\\&=\sum_{m=-\infty}^{\infty}\left[G_1(x_1,x_3;\xi_1,\xi_3+4mh)-G_1(x_1,x_3;\xi_1,-\xi_3+(4m+2)h)\right].\end{aligned} \tag{A.15}$$

Substituting the explicit form of G_1 in terms of the modified Bessel function $K_0(\cdot)$, we obtain

$$\begin{aligned}G_2(x_1,x_3;\xi_1,\xi_3)=\frac{1}{2\pi\epsilon^2}\sum_{m=-\infty}^{\infty}\left[K_0\left(\epsilon^{-1}\sqrt{(x_1-\xi_1)^2+(x_3-\xi_3-4mh)^2}\right)\right.\\\left.-K_0\left(\epsilon^{-1}\sqrt{(x_1-\xi_1)^2+(x_3+\xi_3-(4m+2)h)^2}\right)\right].\end{aligned} \tag{A.16}$$

By construction, at $x_3=\pm h$ the sum of opposite pairs (i.e. m and $-m$) cancel out, thereby enforcing the traction free boundary condition (A.10). Moreover, since the modified Bessel kernel $K_0(\cdot)$ decays exponentially for large arguments, the infinite series converges rapidly for large $|m|$.

So far, we have determined two representations for the Green's function for a strip, namely the Fourier – integral form [Eq. (A.14)] as well as the image – series expansion [Eq. (A.16)]. We now prove that such representations are equivalent, i.e.

$$\begin{aligned}&\sum_{m=-\infty}^{\infty}\left[K_0\left(\epsilon^{-1}\sqrt{(x_1-\xi_1)^2+(x_3-\xi_3-4mh)^2}\right)\right.\\&\left.-K_0\left(\epsilon^{-1}\sqrt{(x_1-\xi_1)^2+(x_3+\xi_3-(4m+2)h)^2}\right)\right]\\&=\int_{-\infty}^{\infty}\frac{\cosh\left\{\beta\left(2h-|x_3-\xi_3|\right)\right\}-\cosh\left\{\beta\left(x_3+\xi_3\right)\right\}}{2\beta\sinh(2\beta h)}e^{-\imath s(x_1-\xi_1)}\mathrm{d}s.\end{aligned} \tag{A.17}$$

To do this, we use the Fourier integral representation of the Bessel function

$$K_0\left(\epsilon^{-1}\sqrt{(x_1-\xi_1)^2+(x_3-\xi_3)^2}\right)=\int_{-\infty}^{\infty}\frac{1}{2\beta}e^{-\imath s(x_1-\xi_1)}e^{-\beta|x_3-\xi_3|}\mathrm{d}s, \tag{A.18}$$

which arises from (A.2) after integrating over η_3 and introducing the transformation $\eta_1=\epsilon s$. Accordingly, the LHS of (A.17) can written as

$$\int_{-\infty}^{\infty}\frac{1}{2\beta}e^{-\imath s(x_1-\xi_1)}\sum_{m=-\infty}^{\infty}\left\{e^{-\beta|x_3-\xi_3-4mh|}-e^{-\beta|x_3+\xi_3-(4m+2)h|}\right\}\mathrm{d}s, \tag{A.19}$$

and making use of the summation formula

$$\sum_{m=-\infty}^{\infty}e^{-\beta|y-4mh|}=\frac{\cosh\left\{\beta(2h-|y|)\right\}}{\sinh 2\beta h},\quad \beta>0,\ |y|<2h, \tag{A.20}$$

the series in the integrand can be evaluated in closed form, giving precisely the RHS in Eq. (A.17).

Finally, if the Green's function $G_2(x_1,x_3;\xi_1,\xi_3)$ in the strip $-h\le x_3\le h$ is employed to represent the non-local stress field as

$$T(x_1,x_3)=\int_{-h}^{h}\mathrm{d}\xi_3\int_{-\infty}^{\infty}G_2(x_1,x_3;\xi_1,\xi_3)\,\sigma(\xi_1,\xi_3)\,\mathrm{d}\xi_1, \tag{A.21}$$

then, by construction, the resulting constitutive boundary condition (CBC) takes the simple form

$$T(x_1,x_3)=0 \text{ at } x_3=\pm h, \tag{A.22}$$

which directly reflects the vanishing property of G_2 at the strip boundaries.

Appendix B. Symmetric and anti-symmetric attenuation functions

The symmetric attenuation function $G_s(\boldsymbol{x},\boldsymbol{\xi})$ is obtained by solving the PDE (A.9) over the half-strip $0\le x_3\le h$, with the mixed boundary conditions

$$G_s(x_1,h,\xi_1,\xi_3)=\frac{\partial G_s}{\partial x_3}(x_1,0,\xi_1,\xi_3)=0, \tag{B.1}$$

and then extending the solution in even fashion for $-h\le x_3<0$, to get

$$\begin{aligned}&G_s(x_1,x_3,\xi_1,\xi_3)=\\&\frac{1}{8\pi\epsilon^2}\int_{-\infty}^{\infty}\frac{\left(e^{-\beta|x_3-\xi_3|}+e^{-\beta|x_3+\xi_3|}\right)\left(e^{2\beta h}-e^{\beta(|x_3-\xi_3|+|x_3+\xi_3|)}\right)}{\beta\left(1+e^{2\beta h}\right)}e^{-\imath s(x_1-\xi_1)}\mathrm{d}s.\end{aligned} \tag{B.2}$$

Similarly, the anti-symmetric attenuation function $G_o(\boldsymbol{x},\boldsymbol{\xi})$ is obtained by solving the PDE (A.9) over the half-strip $0\le x_3\le h$, with the Dirichlet boundary conditions

$$G_o(x_1,h,\xi_1,\xi_3)=G_o(x_1,0,\xi_1,\xi_3)=0, \tag{B.3}$$

and then extending the solution in odd fashion for $-h\le x_3<0$,

$$\begin{aligned}&G_o(x_1,x_3,\xi_1,\xi_3)=\\&\frac{1}{8\pi\epsilon^2}\int_{-\infty}^{\infty}\frac{\left(e^{-\beta|x_3-\xi_3|}-e^{-\beta|x_3+\xi_3|}\right)\left(e^{\beta h}-e^{\beta(|x_3-\xi_3|+|x_3+\xi_3|-h)}\right)}{\beta\sinh(\beta h)}e^{-\imath s(x_1-\xi_1)}\mathrm{d}s.\end{aligned} \tag{B.4}$$

Both kernels G_s and G_o satisfy the point-symmetry (20) and the mirror symmetry (21) conditions.

We now prove the connection (33) between the symmetric/anti-symmetric kernel in the half-strip, $G_{s,o}(\boldsymbol{x},\boldsymbol{\xi})$, and the general kernel in the full strip, $G_2(\boldsymbol{x},\boldsymbol{\xi})$. For this, as in Eq. (34), we write the Green's functions in separated form (to lighten notation, the dependence on x_1 and ξ_1 is omitted)

$$G_{s,o}(x_3,\xi_3)=\begin{cases}F_1(x_3,\xi_3),\ x_3>\xi_3>0,\\F_2(x_3,\xi_3),\ \xi_3>x_3>0,\end{cases} \tag{B.5}$$

and then seek the condition that warrants

$$T(x_3)=\int_{-h}^{h}G_2(x_3,\xi_3)S(\xi_3)\mathrm{d}\xi_3=2\int_{0}^{h}G_{s,o}(x_3,\xi_3)S(\xi_3)\mathrm{d}\xi_3, \tag{B.6}$$

where $T(x_3)$ ($S(x_3)$) is any non-local (local) stress amplitude and we choose G_s (G_o) if $S(x_3)$ is even (odd) in x_3. To fix ideas, we assume $0<x_3<h$, thus

$$\begin{aligned}&2\left\{\int_0^{x_3}F_1(x_3,\xi_3)S(\xi_3)\mathrm{d}\xi_3+\int_{x_3}^{h}F_2(x_3,\xi_3)S(\xi_3)\mathrm{d}\xi_3\right\}\\&=\int_{-h}^{x_3}f_1(x_3,\xi_3)S(\xi_3)\mathrm{d}\xi_3+\int_{x_3}^{h}f_2(x_3,\xi_3)S(\xi_3)\mathrm{d}\xi_3\\&=\int_0^{x_3}\left\{f_1(x_3,\xi_3)S(\xi_3)+f_1(x_3,-\xi_3)S(-\xi_3)\right\}\mathrm{d}\xi_3\\&\quad+\int_{x_3}^{h}\left\{f_2(x_3,\xi_3)S(\xi_3)+f_1(x_3,-\xi_3)S(-\xi_3)\right\}\mathrm{d}\xi_3\\&=\int_0^{x_3}\left\{f_1(x_3,\xi_3)\pm f_1(x_3,-\xi_3)\right\}S(\xi_3)\mathrm{d}\xi_3\end{aligned}$$

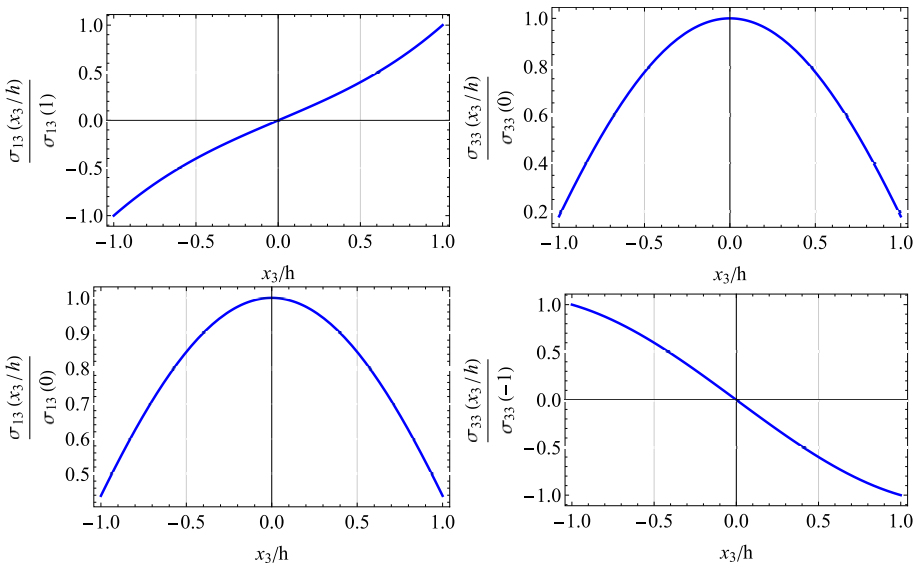

Fig. C.11. Shear (top-left) and transversal (top-right) *local* normalized stress components for the fundamental symmetric mode, and shear (bottom-left) and transversal (bottom-right) local normalized stress components for the fundamental anti-symmetric mode, with dimensionless wavenumber $k_1 = 1$ (having let $\kappa = 1.7$ and $\epsilon_1 = 0.15$).

$$+\int_{x_3}^{h}\left\{f_2(x_3,\xi_3)\pm f_2(-\xi_3,x_3)\right\}S(\xi_3)\mathrm{d}\xi_3, \tag{B.7}$$

where the plus (minus) sign is chosen for $S(x_3)$ even (odd) and we have used reciprocity. Since this equality must hold for *any* function $S(x_3)$ with the relevant symmetry, we obtain the decomposition (33).

Appendix C. Local vs. non-local boundary conditions

Fig. C.11 presents the distribution of the local stress components σ_{13} and σ_{33} for both symmetric and anti-symmetric partial waves. It is clear that the *local* stresses are nonzero at the strip boundaries $x_3 = \pm h$, despite the corresponding *non-local* stresses being identically zero there, in accordance with the imposed BCs. This result contradicts the assumption, adopted by Thi Ngoc Anh et al. (2025), that, given that the non-local stresses vanish at the boundaries, the same should apply to the local stresses. This observation naturally follows from the fact that the differential operator cannot be applied to the BCs, which are valid at a given location.

Appendix D. Non-local stress shorthands

$$\begin{aligned}
P_{11} &= A_1(b_3+k_1\epsilon_1 b_1)e^{k_1 b_1}+A_2(b_3-k_1\epsilon_1 b_1)e^{-k_1 b_1},\\
P_{21} &= A_1\sinh\left(\tfrac{b_3+k_1\epsilon_1 b_1}{\epsilon_1}\right)+A_2\sinh\left(k_1 b_1-\tfrac{b_3}{\epsilon_1}\right),\\
P_{12} &= A_1(b_3-k_1\epsilon_1 b_1)e^{-k_1 b_1}+A_2(b_3+k_1\epsilon_1 b_1)e^{k_1 b_1},\\
P_{22} &= A_1\sinh\left(k_1 b_1-\tfrac{b_3}{\epsilon_1}\right)+A_2\sinh\left(\tfrac{b_3+k_1\epsilon_1 b_1}{\epsilon_1}\right),\\
Q_{11} &= A_3(b_3+k_1\epsilon_1 b_2)e^{k_1 b_2}+A_4(b_3-k_1\epsilon_1 b_2)e^{-k_1 b_2},\\
Q_{21} &= A_3\sinh\left(\tfrac{b_3+k_1\epsilon_1 b_2}{\epsilon_1}\right)+A_4\sinh\left(k_1 b_2-\tfrac{b_3}{\epsilon_1}\right),\\
Q_{12} &= A_3(b_3-k_1\epsilon_1 b_2)e^{-k_1 b_2}+A_4(b_3+k_1\epsilon_1 b_2)e^{k_1 b_2},\\
Q_{22} &= A_3\sinh\left(k_1 b_2-\tfrac{b_3}{\epsilon_1}\right)+A_4\sinh\left(\tfrac{b_3+k_1\epsilon_1 b_2}{\epsilon_1}\right),\\
P_{31} &= A_1\sinh\left(\tfrac{b_3+k_1\epsilon_1 b_1}{\epsilon_1}\right)-A_2\sinh\left(k_1 b_1-\tfrac{b_3}{\epsilon_1}\right),\\
Q_{31} &= A_3\sinh\left(\tfrac{b_3+k_1\epsilon_1 b_2}{\epsilon_1}\right)-A_4\sinh\left(k_1 b_2-\tfrac{b_3}{\epsilon_1}\right),\\
P_{32} &= A_1\sinh\left(k_1 b_1-\tfrac{b_3}{\epsilon_1}\right)-A_2\sinh\left(\tfrac{b_3+k_1\epsilon_1 b_1}{\epsilon_1}\right),\\
Q_{32} &= A_3\sinh\left(k_1 b_2-\tfrac{b_3}{\epsilon_1}\right)-A_4\sinh\left(\tfrac{b_3+k_1\epsilon_1 b_2}{\epsilon_1}\right).
\end{aligned}$$

$$\begin{aligned}
A_{11} &= A_{22} = k_1\epsilon_1 P_1(b_3+k_1\epsilon_1 b_1)e^{k_1 b_1}\\
&+2b_3^2 P_2 e^{\frac{b_3}{\epsilon_1}}\operatorname{cosech}\left(\tfrac{2b_3}{\epsilon_1}\right)\sinh\left(k_1 b_1+\tfrac{b_3}{\epsilon_1}\right),\\
A_{12} &= A_{21} = k_1\epsilon_1 P_1(b_3-k_1\epsilon_1 b_1)e^{-k_1 b_1}\\
&+2b_3^2 P_2 e^{\frac{b_3}{\epsilon_1}}\operatorname{cosech}\left(\tfrac{2b_3}{\epsilon_1}\right)\sinh\left(k_1 b_1-\tfrac{b_3}{\epsilon_1}\right),\\
A_{31} &= A_{42} = k_1\epsilon_1 Q_1(b_3+k_1\epsilon_1 b_2)e^{k_1 b_2}\\
&+2b_3^2 Q_2 e^{\frac{b_3}{\epsilon_1}}\operatorname{cosech}\left(\tfrac{2b_3}{\epsilon_1}\right)\sinh\left(k_1 b_2+\tfrac{b_3}{\epsilon_1}\right),\\
A_{32} &= A_{41} = k_1\epsilon_1 Q_1(b_3-k_1\epsilon_1 b_2)e^{-k_1 b_2}\\
&+2b_3^2 Q_2 e^{\frac{b_3}{\epsilon_1}}\operatorname{cosech}\left(\tfrac{2b_3}{\epsilon_1}\right)\sinh\left(k_1 b_2-\tfrac{b_3}{\epsilon_1}\right),\\
A_{13} &= -A_{24} = (b_3 P_3-k_1\epsilon_1 P_2)\sinh\left(k_1 b_1+\tfrac{b_3}{\epsilon_1}\right),\\
A_{14} &= -A_{23} = (b_3 P_3+k_1\epsilon_1 P_2)\sinh\left(k_1 b_1-\tfrac{b_3}{\epsilon_1}\right),\\
A_{33} &= -A_{44} = (b_3 Q_3-k_1\epsilon_1 Q_2)\sinh\left(k_1 b_2+\tfrac{b_3}{\epsilon_1}\right),\\
A_{34} &= -A_{43} = (b_3 Q_3+k_1\epsilon_1 Q_2)\sinh\left(k_1 b_2-\tfrac{b_3}{\epsilon_1}\right).
\end{aligned}$$

Data availability

No data was used for the research described in the article.

References

Achenbach, J., 2012. Wave Propagation in Elastic Solids. Elsevier.

Chandrasekharaiah, D., 1987. Rayleigh-lamb waves in an elastic plate with voids. J. Appl. Mech. 54 (3), 509–512.

Eringen, A.C., 1972. Linear theory of nonlocal elasticity and dispersion of plane waves. Internat. J. Engrg. Sci. 10 (5), 425–435.

Eringen, A.C., 1983. On differential equations of nonlocal elasticity and solutions of screw dislocation and surface waves. J. Appl. Phys. 54 (9), 4703–4710.

Eringen, A.C., 1984. Theory of nonlocal elasticity and some applications. Civil Engng.Res. Rep. No. 84-SM-9 62.

Eringen, A.C., 2002. Nonlocal Continuum Field Theories. Springer-Verlag, New York.

Eringen, A.C., Edelen, D., 1972. On nonlocal elasticity. Internat. J. Engrg. Sci. 10 (3), 233–248.

Eringen, A.C., Kim, B.S., 1974. Stress concentration at the tip of crack. Mech. Res. Commun. 1 (4), 233–237.

Graff, K.F., 2012. Wave Motion in Elastic Solids. Courier Corporation.

Kaplunov, J., Prikazchikov, D., Prikazchikova, L., 2022. On non-locally elastic Rayleigh wave. Phil. Trans. R. Soc. A 380 (2231), 20210387.

Kaplunov, J., Prikazchikov, D.A., Prikazchikova, L., 2023. On integral and differential formulations in nonlocal elasticity. Eur. J. Mech. A Solids 100, 104497.
Karlicic, D., Murmu, T., Adhikari, S., McCarthy, M., 2015. Non-Local Structural Mechanics. John Wiley & Sons.
Kaur, G., Singh, D., Tomar, S., 2021. Lamb waves in nonlocal elastic plate with voids. J. Mech. Mater. Struct. 16 (4), 389–405.
Kröner, E., 1967. Elasticity theory of materials with long range cohesive forces. Int. J. Solids Struct. 3 (5), 731–742.
Kumar, S., Tomar, S., 2022. Lamb waves in elastic–plastic plate containing voids. IMA J. Appl. Math. 87 (3), 438–461.
Kuznetsov, S., 2014. Lamb waves in anisotropic plates. Acoust. Phys. 60 (1), 95–103.
Lamb, H., 1917. On waves in an elastic plate. Proc. R. Soc. Lond. Ser. Contain. Pap. Math. Phys. Character 93 (648), 114–128.
Melnikov, Y.A., Melnikov, M.Y., 2012. Green's Functions: Construction and Applications, vol. 42, Walter de Gruyter.
Mindlin, R., 1960. Waves and vibrations in isotropic, elastic plates. Struct. Mech. 199–232.
Nobili, A., 2021. Asymptotically consistent size-dependent plate models based on the couple-stress theory with micro-inertia. Eur. J. Mech. A Solids 89, 104316.
Nobili, A., Erbaş, B., Signorini, C., 2022. Veering of Rayleigh–lamb waves in orthorhombic materials. Math. Mech. Solids 27 (9), 1783–1799.
Nobili, A., Pramanik, D., 2025a. Indeterminacy and well-posedness of the non-local theory of Rayleigh waves. Internat. J. Engrg. Sci. 216, 104321.
Nobili, A., Pramanik, D., 2025b. A well-posed theory of linear non-local elasticity. Internat. J. Engrg. Sci. 215, 104314.
Nobili, A., Radi, E., Signorini, C., 2020. A new Rayleigh-like wave in guided propagation of antiplane waves in couple stress materials. Proc. R. Soc. A 476 (2235), 20190822.
Pham, C.V., Vu, T.N.A., 2024. On the well-posedness of eringen's non-local elasticity for harmonic plane wave problems. Proc. R. Soc. A 480 (2293), 20230814.
Pramanik, D., Nobili, A., 2025. A well-posed non-local theory in 1D linear elastodynamics. Int. J. Solids Struct. 113511.
Royer, D., Clorennec, D., Prada, C., 2009. Lamb mode spectra versus the Poisson ratio in a free isotropic elastic plate. J. Acoust. Soc. Am. 125 (6), 3683–3687.
Ryden, N., Park, C.B., Ulriksen, P., Miller, R.D., 2003. Lamb wave analysis for non-destructive testing of concrete plate structures. In: 16th EEGS Symposium on the Application of Geophysics To Engineering and Environmental Problems. European Association of Geoscientists & Engineers, pp. cp–190.
Solie, L., Auld, B., 1973. Elastic waves in free anisotropic plates. J. Acoust. Soc. Am. 54 (1), 50–65.
Thi Ngoc Anh, V., Vinh, P.C., Tuan, T.T., 2025. Transfer matrix for a weakly nonlocal elastic layer and lamb waves in layered nonlocal composite plates. Math. Mech. Solids 30 (3), 628–640.
Zima, B., Kędra, R., 2020. Numerical study of concrete mesostructure effect on lamb wave propagation. Materials 13 (11), 2570.